SCM-SS Scheme for Optical MIMO Transmission Over Multimode Fiber Links

Yang Zhang

Electronic and Photonic Systems Engineering

A thesis submitted for the degree of PhD

February, 2014

Abstract

Today's optical fiber communication systems employ time division multiplexing (TDM), wavelength division multiplexing (WDM), and polarization division multiplexing (PDM) to carry as much traffic as possible. Due to the rapid spread of Internet services, demand for large transmission capacity has been increasing exponentially. It is imperative to resort to other physical dimensions to fulfill the greedy capacity demand.

Optical multiple-input multiple-output (MIMO) exploits the space domain, it allows simultaneous transmission of multiple channels, therefore enhances the network capacity. Utilizing multicore fiber is so called space division multiplexing (SDM). Taking advantage of the inherent modes of few-mode or multimode fiber can be defined as mode division multiplexing (MDM). They have the potential of higher transport capacity limit than single mode fibers (SMF).

However, there are formidable technical challenges in high capacity SDM.

Optical MIMO with coherent detection needs local oscillators at the receiver side to keep a linear down conversion process of the optical fields. The cost would be prohibitive for low cost systems. Direct detection is eminently practical and cost-effective.

An MDM transmission scheme called subcarrier multiplexing with spread spectrum (SCM-SS) is proposed. SCM is to produce a modulated single sideband with an optical carrier, which can be self-heterodyned through square-law detection. Moreover it is

ABSTRACT

able to relieve the impairment of chromatic dispersion. Spread spectrum technique is to spread the spectrum of the optical field created by SCM. SCM is realized by using dual-drive Mach-Zehnder modulator (MZM) and 90° hybrid coupler. Spectrum is broadened by direct sequencing (DS).

Its feasibility and performance are confirmed theoretically, numerically and experimentally. Up to 2000 m transmission with multiple spans of fibers was demonstrated. Detailed comparisons are made between SCM-SS, SCM and IMDD-SS.

Contents

Chapter 1

Introduction

1.1 Background

Since its debut, optical communications have played an important role in transporting worldwide data and voice traffic in volume. Data-centric cloud services may accelerate the growth rate. The explosive traffic growth has sparked the development of a number of important technologies. Conventional time division multiplexing (TDM), wavelength division multiplexing (WDM), code division multiplexing (CDM), and polarization division multiplexing (PDM) have increased the capacity of a lightwave system drastically, though, the greedy capacity demands still frustrate the industry [1]. Inasmuch as aforementioned multiplexing schemes are striving to achieve their scalability limits, it is imperative to resort to other physical dimensions.

1.2 Optical MIMO

Optical MIMO is devoted to exploiting the space domain. Although it seems daunting and challenging, the great potential of capacity and telling prospects have generated

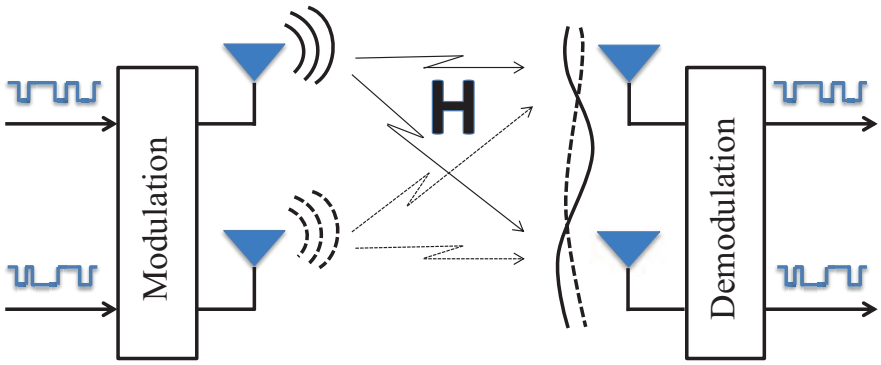

(a) Schematic of wireless MIMO.

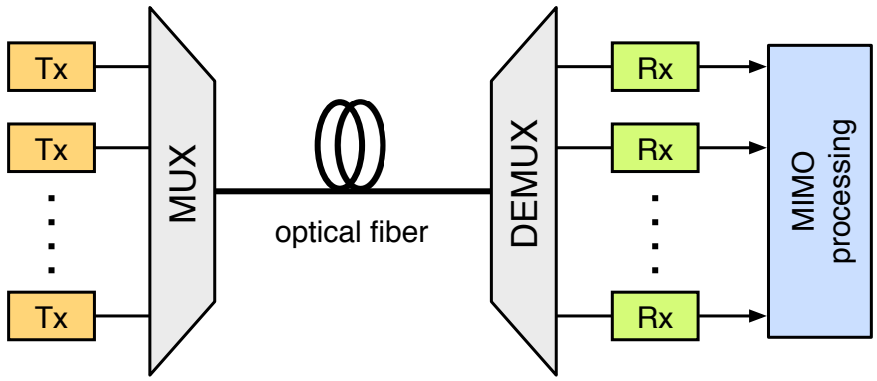

(b) Schematic of optical MIMO.

Figure 1.1 Wireless MIMO versus optical MIMO.

much interest among researchers. Transmission over multicore fibers is coined as space division multiplexing (SDM), on the other hand, mode division multiplexing (MDM) takes advantage of few-mode or multimode fibers. The concept of MIMO was first introduced in wireless communications since the seminal paper of Foschini and Gans [2]. Dramatic increases in capacity and reliability of wireless links are achieved by using multiple antennas at transmitter and/or receiver ends, as shown in Figure 1.1(a). The benefit of MIMO is profound. MIMO technology is a promising tool for enabling spectrally efficient future applications, and can combat severe channel fading and distortions. Optical MIMO is based on the analogy between multipath fading in wireless

channels and multiple light propagation paths within optical fibers, which allows transmission of multiple data channels simultaneously through a single fiber, as shown in Figure 1.1(b). Nevertheless, the distinguishments between optical and wireless MIMO are pronounced. Wireless MIMO supplies a growing capacity by exploiting the multipath nature of wireless channels. In wireless MIMO, the output voltage or current from each receive antenna is proportional to the received field amplitude. However, in the optical case, the photocurrent is rather proportional to the square of the field envelope. Because of the quadratic nature of photo detection, MIMO techniques in wireless communication may not be applied to optical transmission directly, leaving us much challenging work to do.

1.2.1 Space division multiplexing (SDM)

Space division multiplexing is one of the candidate technologies to cope with the increasing traffic, which takes advantage of multicore fibers. Multicore fiber consists of multiple cores arranged in a hexagonal array and is fabricated using the stack and draw process.

Recently, various new types of multicore fiber and transmission results based on SDM have been reported [3]–[17]. Multicore fiber links require great precision in multiplexing and demultiplexing based on free-space optical configuration [16], [17], or specially designed tapered multicore fiber connector [18]. There are formidable technical challenges in coupling signals into and out of each core in multicore fiber because the cores are closely spaced. Successful development of multicore fiber as a competing technology to existing systems requires dealing with a number of technical obstacles, including crosstalk [15]. It is very difficult to design and manufacture high-core-count, low-loss, and low-crosstalk multicore fiber. Random perturbations play a crucial role in

determining the crosstalk in multicore transmission fibers [19]. To transmit signals independently on each core, suppression of intercore crosstalk has been a primary concern in multicore fiber research for high-capacity long-distance transmissions.

1.2.2 Mode division multiplexing (MDM)

Mode division multiplexing takes advantage of few-mode or multimode fibers. Inside few-mode or multimode fibers, multiple modes can exist at the operating wavelength, as is pictorially illustrated in Figure 1.2.

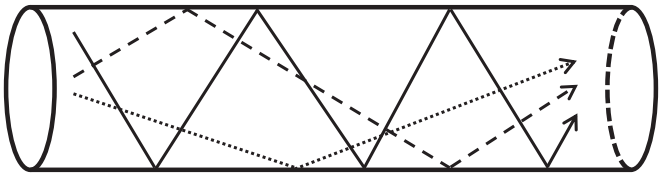

Figure 1.2 Multiple modes exist inside few-mode or multimode fibers at the operating wavelength.

The *modes* are field distributions that are solutions of Maxwell's equations. Each mode is associated with a particular group delay. There are no crucial distinctions between few-mode fiber and multimode fiber. It is merely that only a few modes can be supported in few-mode fiber, whereas there are hundreds of in multimode fiber. Few-mode fibers are demonstrated as a good compromise, since they are sufficiently resistant to mode coupling compared to standard multimode fibers, but they still can have large core diameters compared to single mode fibers. Mode division multiplexing is currently attracting much interest among researchers [4], [8], [13], [20]–[30]. Compared to space division multiplexing, mode division multiplexing would relax the requirement of fiber manufacturing. Moreover, mode division multiplexing has higher space utility efficiency. Therefore, it is much more cost-effective.

1.3 Detection methods for optical MIMO

From a practical point of view, either coherent detection or direct detection can be employed in optical MIMO system. A main differentiating aspect of optical communication systems is the receiver type, be it direct detection, or homodyne/heterodyne coherent detection. There are distinctive features between coherent detection system and direct detection system.

1.3.1 Coherent detection

Coherent detection requires local oscillators at the receiver side to keep a linear down conversion process, exacerbating complexity and cost significantly. Coherent detection results in photocurrent components directly proportional to the quadrature components of the optical field complex amplitude, rendering coherent optical system formally equivalent to wireless MIMO. A number of mode division multiplexing proposals have been reported based on coherent detection [21], [22], [31].

1.3.2 Direct detection

Direct detection obviates the need to set local oscillators at the receiver side, hence simplifies the system configuration. Optical MIMO with direct detection is quite different from that with coherent detection. MDM implementations based on direct detection have been reported extensively [32]. Direct detection is preferable concerning the practical realization and cost. However, due to fiber imperfections, bends, perturbations, [33], mode coupling would happen within the fiber, incurring harmful cross terms upon square-law detection. A variety of countermeasures have been presented to deal with the impairment induced by mode coupling. An optical method called mode-selective spatial filtering was proposed in [34] to reduce the spatial overlap among the

fields of detected mode groups. A few-mode transmission fiber with low mode coupling was reported in [35], which can be used as a key component for mode division multiplexing.

1.4 Outline of the thesis

Optical MIMO is an attractive way to improve the capacity of fiber-optic links by exploiting the space domain. Mode division multiplexing is the main concern of this research. The purpose is to reach practical solution that enable the efficient design and applicability of a mode division multiplexing system. There are obstacles for utilizing the modes inside fibers, such as mode coupling, laser phase noise, etc. In order to overcome these problems, a direct detection implementation called subcarrier multiplexing with spread spectrum (SCM-SS) scheme for optical MIMO transmission is proposed.

Chapter 2 is concerned with the theoretical principle of SCM-SS scheme. Communication channels of this system are first investigated. Existing solutions for mode division multiplexing are briefly reviewed, their main characteristics, especially drawbacks are analyzed. To tackle mode coupling induced impairments, spread spectrum techniques are incorporated in the system. Signal propagation in narrowband scenario and wideband scenario are elucidated in detail. MIMO digital signal processing algorithms are done offline to retrieve original transmitted data.

More specifically, Chapter 3 numerically investigates the transmission over nondispersive channel and over dispersive channel respectively. Both simulated transmission and experimental transmission have been demonstrated.

In Chapter 4, experimental transmissions of SCM-SS scheme over multimode fiber links are demonstrated. Practical realization of SCM-SS scheme is verified. 2×2, 2×4,

4×4 transmission are demonstrated.

In Chapter 5, conclusions are drawn, outlooks and perspectives are given. Achievements of this research are summarized, and the promises and challenges of such systems are explored.

Chapter 2

SCM-SS scheme

As discussed in the preceding chapter, mode division multiplexing with direct detection is a promising solution for cost-effective optical MIMO transmission. However, there are numerous problems need to be coped with. In this chapter, SCM-SS scheme is introduced. The characteristics of the communication channels are analyzed. Spread spectrum techniques are introduced and the application in energy density reduction is emphasized. For wideband channels, self-interference would degrade the system drastically. MIMO digital signal processing algorithms are demonstrated.

2.1 Communication channels

2.1.1 Issues related to fiber channels

Choice of fiber types

The communication channels for mode division multiplexing are few-mode or multimode fibers. Multimode fibers are widely used in current high-speed, low-cost local area networks (LANs). Compared to space division multiplexing that using multicore

fibers, mode division multiplexing is emerging as an attractive solution for the required capacity increase with potential cost, space, and energy savings. LANs are traditionally based on multimode fibers because of looser alignment tolerances compared to single mode fibers. Because few-mode or multimode fibers.

Fiber modes

The concept of the mode is a general concept in optics occurring also, for example, in the theory of lasers. A *mode* refers to a specific solution of the wave equation that satisfies the appropriate boundary conditions and has the property that its spatial distribution does not change with propagation. The fiber modes can be classified as guided modes, leaky modes, and radiation modes. Signal transmission in fiber-optic communication systems takes place through the guided modes only.

A specific spectral component at the frequency ω would arrive at the output end of the unit length fiber after a time delay $\tau = 1/v_g$, where v_g is the *group velocity*, defined as

$$v_g = (d\beta/d\omega)^{-1} \tag{2.1}$$

where β is the *propagation constant*. Each mode is associated with its particular propagation constant. Different modes propagate with different group velocities, inducing a phenomenon called *modal dispersion*. Multimode fiber features that multiple modes exist inside the fiber at the operating wavelength.

Wave propagation

The mode power distribution (MPD) determines the modes propagating along the fiber. The MPD can be controlled by the launching conditions. The *coupling efficiency* ξ represents how the mode of the incident light "couples" or is "accepted" into a fiber.

It is the fraction of the power of the incident optical field mode that is coupled into the propagation mode of the fiber, and is computed by overlap integrals

$$\xi_{lp} = \frac{|\iint \mathbf{E}_i(x,y)\mathbf{E}^*_{lp}(x,y)dxdy\,|^2}{\iint |\mathbf{E}_i(x,y)|^2 dxdy \iint |\mathbf{E}_{lp}(x,y)|^2 dxdy} \tag{2.2}$$

A field distribution at the beginning of the fiber will mainly excite mode with a similar mode field distribution. Center launching with a single mode fiber will almost excite the fundamental mode, while offset launching will distribute the power mainly within higher order modes.

Degradation

Multimode fiber links suffer from a variety of impairments that would degrade the system performance. Although different modes have the potential of carrying multi-channels, the coupling of different modes always occurs in multimode fiber, and is inevitable during transmission. Intermodal coupling should be taken into consideration in transmission system design. When multiple channels involved, they will interfere with each other, and because of the quadratic nature of photo detection, cross-product terms would emerge in the received electrical signals besides the information-bearing RF components, making it difficult to divide each channel. Fiber losses depend on the wavelength of transmitted light. Spatial mode filtering increase modal noise and degrade channel performance.

2.1.2 Fast fading and slow fading channels

Channel varying in time is said to be *fading*, also known as *scintillation*, which severely degrades the link performance. The channel variations or fades are due to physical changes in the propagation medium. According to the duration of *codeword* relative to the channel variations, fast fading and slow fading are defined. Channel *coherence*

time is a useful measure to characterize the behavior of fading channels. In short, the coherence time is the time duration before a channel varies significantly. In a fast fading channel, the *coding delay* is much larger than the coherence time. The channel varies very fast so that the coding horizon spans many channel fades. In a slow fading channel, the coding delay is much smaller than the coherence time. Therefore, the channel is assumed to remain constant over the duration of a codeword. It is important to understand the difference between a fast fading channel and a slow fading channel, for which the treatments are quite distinct. Due to a number of factors such as inhomogeneity in the pressure and temperature fluctuations, it is unlikely for fiber channels to keep stable. The variation rate of fiber channel is much smaller than the data rate, which is hence categorized into slow fading channel.

2.1.3 Narrowband and wideband channels

For multipath fading channels, multipath components arriving at different delay times correspond to various routes between the transmitter and receiver. These different routes have different lengths and therefore the signal components are expected to arrive at the receiver with different delays. Narrowband and wideband are relative notions. A narrowband channel is that all the multipath components arrive with delays that are very close to each other relative to symbol duration. A wideband channel is that the temporal extent of the multipath components is comparable to the symbol duration, the effect of previously transmitted symbols would superimpose on the current symbol because of delayed copies, which is known as *intersymbol interference* (ISI). Narrowband channel is also referred to as *frequency flat* channel, and wideband channel is called *frequency selective* channel.

The metric of delay spread in multimode fiber is *differential mode delay* (DMD).

DMD measurements are used to calculate the effective modal bandwidth (EMBc), which is an alternative method for characterizing fiber performance.

2.2 Existing solutions for MDM

An overall understanding on the communication channels of mode division multiplexing laid the foundation of exploiting them. We have seen a number of important developments in the context of mode division multiplexing. The main goal of this thesis is to conceive a direct detection implementation for mode division multiplexing, therefore solutions with coherent detection are out of the scope of concerning.

2.2.1 Baseband signaling

The simplest signaling scheme for optical MIMO is intensity modulation direct detection (IMDD). Solutions in baseband signaling scenario have been reported by some researchers [22], [36]. The basic idea behind IMDD is a linear input-output relationship with respect to intensity. Techniques such as mode group division multiplexing (MGDM) claimed that a linear relation was held between input and output with respect to the optical intensity by assuming negligible intermodal coupling [37]. By considering low mode coupling, mode groups propagate nearly independently and can be separated by spatially resolved receivers. However, independent propagation of mode groups inside fiber seems to be rather challenging in praxis [38]. MGDM claims linear real-valued transmission matrix with respect to the optical intensity by assuming negligible intermodal coupling, therefore the channel matrix should be diagonally dominant. In other words, real-valued channel matrix requires the diagonal elements have larger values than rest of the elements, in order to keep in small condition number. When multiple fields from different channels overlap, cross product terms would surely arise.

2.2.2 Passband signaling

Passband signaling strategies include subcarrier multiplexing (SCM) [39], orthogonal frequency division multiplexing (OFDM) [20], [23], [24], [40], etc. These schemes port known techniques from wireless communication to multimode fiber transmission, overcoming modal dispersion by signaling in parallel over multiple frequency disjoint orthogonal channels. Unfortunately, in optical transmission, one has to contend with mitigating the second-order intermodulation between the subcarriers.

2.3 Spread spectrum techniques

The initial application of spread spectrum techniques was in the development of military guidance and communication systems, and during subsequent years, there emerged an assortment of other applications in such areas as energy density reduction, high-resolution ranging, and multiple access. It is called *spread spectrum* because the transmission bandwidth employed is much greater than the minimum bandwidth required to transmit the information. Spreading is accomplished by means of a *spreading signal*, often called a *code signal*, which is independent of the data. In digital communications, a *chip* is a pulse of a direct-sequence spread spectrum (DSSS) code, such as a pseudo-noise code sequence used in direct-sequence code division multiple access (CDMA) channel access techniques. The *chip rate* of a code is the number of pulses per second (chips per second) at which the code is transmitted (or received). The chip rate is larger than the symbol rate, meaning that one symbol is represented by multiple chips. *signature* If we define $T_b = 1/R$ to be the duration of a rectangular pulse corresponding to the transmission time of an information bit, the ratio of the chip rate to the information

bit rate may be expressed as

$$B_e = \frac{W}{R} = \frac{T_b}{T_c} \tag{2.3}$$

B_e is called *spreading factor*, *bandwidth expansion factor* or *processing gain*.

Resolvable multipath components resulting from time-dispersive propagation through a channel may be viewed as a form of *self-interference*. results in a reduction of by a factor of across the spread spectrum. The generators generate which is impressed on the transmitted signal at the modulator and removed from the received signal at the demodulator. After time synchronization of the generators is established, the transmission of information may commence. Interference is introduced in the transmission of the information-bearing signal through the channel. The characteristics of the interference depend to a large extent on its origin. It may be categorized as being either narrowband or wideband relative to the bandwidth of the information-bearing signal. The PN sequence generated at the modulator is used in conjunction with the PSK modulation to shift the phase of the PSK signal pseudorandomly. The resulting modulated signal is called a *direct sequence* (DS) or a *pseudo-noise* (PN) spread spectrum signal. When used in conjunction with binary or M-ary ($M > 2$) FSK, the pseudorandom sequence selects the frequency of the transmitted signal pseudorandomly. The resulting signal is called a *frequency hopped* (FH) spread spectrum signal. The two common spread spectrum techniques are direct sequence (DS) and frequency hopping (FH).

2.4 Principle of SCM-SS scheme

In the previous discussion, we get to know that the problem is intractable when mode coupling occurs, be it baseband signaling, or passband signaling. Notwithstanding, the energy density reduction ability of spread spectrum techniques sparked the possi-

ble application in mode division multiplexed optical MIMO systems. Hereof, a direct detection implementation called SCM-SS scheme for optical MIMO transmission is proposed. The basic idea of SCM-SS scheme is to overcome intermodal coupling incurred impairment in direct detection regime.

2.4.1 Architecture

The architecture of SCM-SS scheme is depicted in Figure 2.1. Transmitter of each

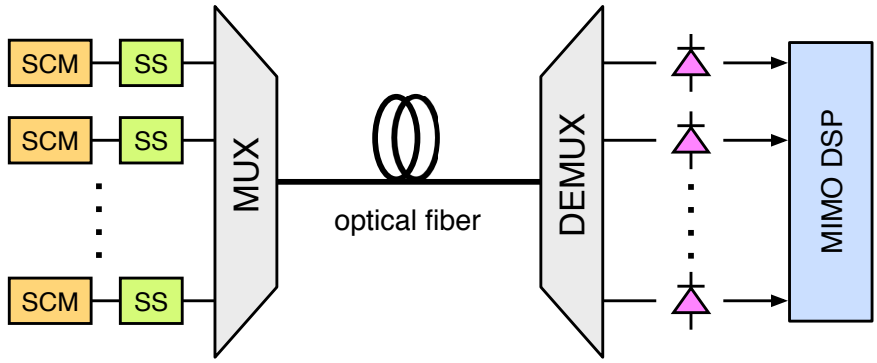

Figure 2.1 Architecture of SCM-SS scheme.

channel consists of subcarrier multiplexing (SCM) and spread spectrum (SS) modulation, denoted as SCM-SS. The motivation of SCM is to produce a modulated single sideband with an optical carrier, which can be self-heterodyned through square-law detection, moreover it is able to relieve the impairment of chromatic dispersion. The optical spectrum created by SCM is conceptually shown in Figure 2.2. Spread spectrum modulation is to phase modulate the optical field created by SCM with a sequence of spectrum-spreading code, herein each channel is assigned a unique signature. In the following discussions, narrowband scenario and wideband scenario are dealt with distinctively.

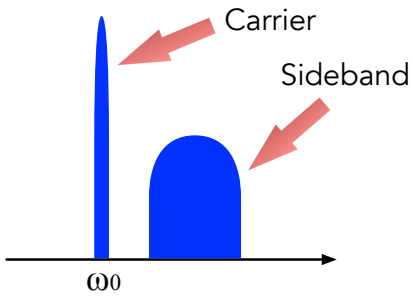

Figure 2.2 Optical spectrum created by SCM. ω_0 is the optical carrier frequency.

2.4.2 Narrowband scenario

Narrowband scenario is when optical waves undergo modal dispersion within one chip duration. Assume a MIMO system consisting of N_t transmitters and N_r receivers. The optical field of each channel at the multimode fiber input side can be expressed as

$$E_j(t) = \exp\Big(i\omega_0 t + i\phi_j(t) + ic_j(t)\Big)\Big\{A_0 + A_m \exp\Big(i\omega_m t + i\varphi_j(t)\Big)\Big\} \tag{2.4}$$

where $j = 1, 2, \ldots, N_t$. ω_0 is the optical carrier, ω_m is the RF subcarrier, $\phi_j(t)$ is the laser phase noise, $c_j(t)$ is the spreading code induced phase changing, $\varphi_j(t)$ is the phase shift keyed (PSK) data, A_0 and A_m are amplitude of optical carrier and that of the sideband respectively.

Since different modal power distributions are excited by different channels at the fiber input facet, each channel will experience a different propagation procedure, that is, carried by different set of modes with different fractions of power, until arriving at the receiver side. At the receiver side, every detector receives a collection of optical fields from different channels, attempts of decomposing channels in optical domain are

not needed. Optical field impinged on the ith photo detector can be expressed as

$$\begin{aligned} U_i(t) &= \sum_{j=1}^{N_t} E_j(t) * g_{ij} \\ &= \sum_{j=1}^{N_t} E_j(t) * \sum_{k=1}^{P} a_{ijk}\, \delta(t-\tau_k) \\ &= \sum_{j=1}^{N_t} \sum_{k=1}^{P} a_{ijk}\, E_j(t-\tau_k) \end{aligned} \tag{2.5}$$

where $i = 1, 2, \ldots, N_r$. $*$ means convolution, g_{ij} is the impulse response associated with ith receiver and jth transmitter, P is the number of modes supported by multimode fiber channel, a_{ijk} is a multiplicative factor, the subscript ijk means from the jth transmitter, via the kth mode, to the ith receiver, and τ_k is the group delay for the kth mode. The square-law-detected photo current, exclusive of dc component and additive noise, is described as

$$r_i(t) = \sum_{j=1}^{N_t} A_{ij} \cos\Big(\omega_m t + \varphi_j(t) + \theta_{ij}\Big) + \text{s.i.} \tag{2.6}$$

where A_{ij} is the resultant amplitude of RF signal from the jth transmitter to the ith receiver, θ_{ij} is the resultant phase in RF subcarrier. Since each channel experienced a different propagation procedure, time delay τ_k was translated into a phase delay $\omega_m \tau_k$, θ_{ij} is apt to be different for each transmitter/receiver pair, in other words, we may take benefit from the multipath scattering environment provided by multimode fiber [31], and s.i. represents suppressed impairment. Look back at Equation (2.4), the phase noise $\phi_j(t)$ in optical carrier of each channel using individual laser behaves independently. Providing optical fields of different channels coupled together, see Figure 2.3, upon square-law detection, the interaction of phase noises would also appear in RF band, along with the information-bearing RF signals, see Figure 2.4(a). The impairment from laser phase noises may totally corrupt the transmission. By employing the spread spectrum technique, the phase noise induced impairment is spectrally broadened, so

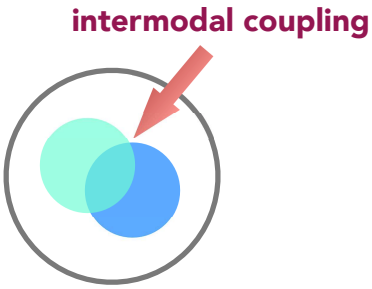

Figure 2.3 Two channels coupled together.

the power of phase noise containing terms in-band are dramatically suppressed, see Figure 2.4(b).

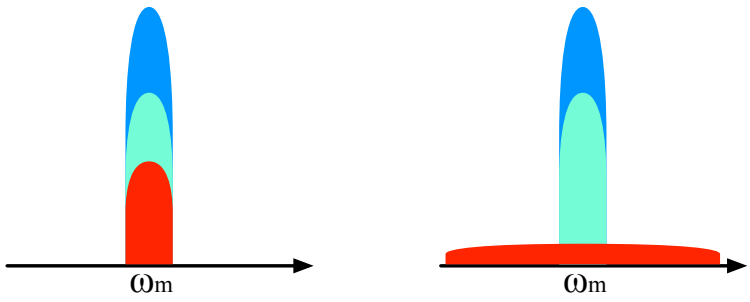

Figure 2.4 ■ Signal from Channel 1. ■ Signal from Channel 2. ■ Impairment. ω_m is the RF subcarrier frequency. (a) Electrical spectrum without spread spectrum technique. (b) Electrical spectrum with spread spectrum technique.

In the context of IMDD implementation, spatial overlap among fields of different channels should be reduced as much as possible in order to keep a linear relation with respect to optical intensity, otherwise with the advent of cross terms, it is unable to compensate for interferences among channels by MIMO signal processing. Spread spectrum techniques can be incorporated in IMDD to suppress cross terms, though, phase modulated constellations are not supported in the absence of subcarrier.

2.4.3 Wideband scenario

Wideband scenario is when optical waves undergo modal dispersion beyond one chip duration. Consider a DS BPSK communication system operating over a multipath channel that has more than one path from the transmitter to the receiver. The different paths consist of several discrete paths each with a different attenuation and time delay. Figure 2.4(b) illustrates a communication link with two discrete paths. The multipath wave is delayed by some time τ, compared with the direct wave. Under extreme conditions, such signals may cause complete loss of synchronization.

In a direct-sequence spread spectrum system, if we assume that the receiver is synchronized to the time delay and RF phase of the direct path, the received signal can be expressed as

$$r(t) = Ax(t)g(t)\cos\omega_0 t + \alpha Ax(t-\tau)g(t-\tau)\cos(\omega_0 t + \theta) + n(t) \tag{2.7}$$

where $x(t)$ is the data signal, $g(t)$ is the code signal, $n(t)$ is a zero-mean Gaussian noise process, and τ is the differential time delay between the two paths, assumed to be in the interval $\theta < \tau < T$. The angle θ is a random phase, assumed to be uniformly distributed in the range $(0, 2\pi)$, and α is the attenuation of the multipath signal relative to the direct path signal. For the receiver, synchronized to the direct path signal, the output of the correlator can be written as where $g^2(t) = 1$. Also, for $\tau > T_c$, $g(t)g(t-\tau) \approx 0$ (for codes with long periods), where T_c is the chip duration. Therefore, if T_c is less than the differential time delay between the multipath and direct path signals, we can write where $n_0(T)$ is a zero-mean Gaussian random variable. We can see that the spread-spectrum system, similar to the case of CDMA, effectively eliminates the multipath interference by virtue of its code-correlation receiver.

2.5 MIMO digital signal processing

MIMO digital signal processing is done offline to retrieve the transmitted data. The flow chart of MIMO digital signal processing is depicted in Figure 2.5.

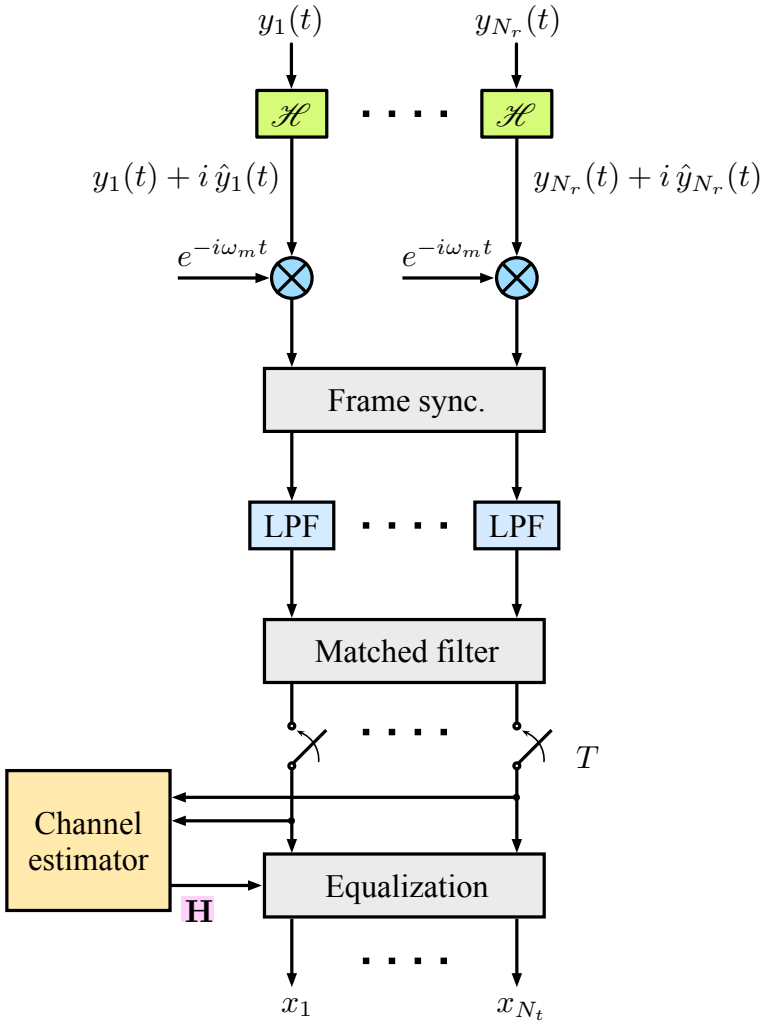

Figure 2.5 Flow chart of MIMO digital signal processing.

2.5.1 Lowpass equivalent

The ubiquitous rule is to work with the lowpass equivalents of bandpass signals instead of directly working with them. That is so because applying signal processing algorithms

to lowpass signals is much easier. The real-valued bandpass signal in Equation (2.6) is turned to complex lowpass equivalent through Hilbert transform

$$y_i(t) = \Big(r_i(t) + i\,\hat{r}_i(t)\Big)e^{-i\omega_m t} \tag{2.8}$$

where $\hat{r}_i(t) = r_i(t) * (1/\pi t)$ is the Hilbert transform of $r_i(t)$. $r_i(t) + i\,\hat{r}_i(t)$ is called the *analytic signal* or *pre-envelope* of $r_i(t)$. $y_i(t)$ is the *lowpass equivalent* of $r_i(t)$. Hereby the RF subcarrier is removed.

2.5.2 Frame synchronization

All digital communication systems require some degree of synchronization to incoming signals by the receivers. Almost all digital data streams have some sort of frame structure. This is to say that the data stream is organized into uniformly sized groups of bits. For a receiver to make sense of the incoming data stream, the receiver needs to be synchronized with the frame structure of data stream. Frame synchronization is accomplished with the aid of *frame marker*. The frame marker is a short pattern of bits that the transmitter injects periodically into the data stream. Detection of the frame marker would indicate a known position (typically the beginning) in the data frame. One *frame* consists of training sequence and the following data, as shown in Figure 2.6. All the channels are frame synchronized, and each channel is allocated

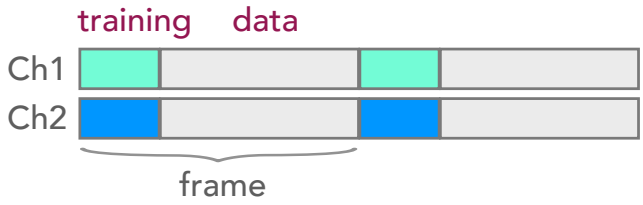

Figure 2.6 Frame structure.

with a unique training sequence. The training sequence can suffice as a frame marker.

The frame structure is known by both the transmitter and receiver. Receiver generates frame marker replica, which is correlated with the incoming data stream

$$C(\tau) = \Big|\mathbf{E}\big[x(t)\, y^*(t+\tau)\big]\Big| \tag{2.9}$$

where $x(t)$ is the generated frame marker replica, $y^*(t+\tau)$ is the conjugate of the time-shifted version of $y(t)$, and $C(\tau)$ is the cross correlation between frame marker and data stream. When the receiver comes into frame synchronization, each data stream is passed through a lowpass filter to eliminate broadband additive noises.

2.5.3 Matched filter

The matched filter assumes that perfect or nearly perfect symbol synchronization has been achieved. And this requirement is fulfilled by the previous step of frame synchronization. The lowpass equivalent of each received data stream is applied to a matched filter. And the output of matched filter is sampled at the end of each symbol interval. As a result, the sampled (at symbol rate) lowpass equivalent corresponding to the ith receiver can be expressed as a linear combination of transmitted symbols

$$y_i = \sum_{j=1}^{N_t} \alpha_{ij}\, e^{i\theta_{ij}} \cdot x_j + n_i \tag{2.10}$$

where α_{ij} is the sampled amplitude, x_j is the symbol from the jth transmitter, n_i is the additive noise. For mathematical convenience, Equation (2.10) can be represented in matrix form as

$$\mathbf{y} = \mathbf{H}\mathbf{x} + \mathbf{n} \tag{2.11}$$

where $\mathbf{y} = [\, y_1\ y_2\ \ldots\ y_{N_r}\,]^T$, $\mathbf{x} = [\, x_1\ x_2\ \ldots\ x_{N_t}\,]^T$, $\mathbf{H}$ is channel matrix with complex entries of h_{ij}, and $\mathbf{n}$ accounts for noises. The variation rate of fiber channel is much smaller than the data rate, which is hence categorized into slow fading channel. The

perception of **H** relies on channel estimation algorithms, which are introduced in the following.

2.5.4 Channel estimation

The information available about the channel is called channel state information (CSI). There are basically two levels of CSI, namely instantaneous CSI and statistical CSI. In slow fading systems instantaneous CSI can be estimated with reasonable accuracy. On the other hand, in fast fading systems where channel conditions vary rapidly under the transmission of a single information symbol, only statistical CSI is reasonable, which is outside the scope of this topic. Since the channel conditions vary, instantaneous CSI needs to be estimated on a short-term basis using the combined knowledge of the transmitted and received signals. Channel estimation can be performed through reorganizing the system model equation as follows

$$\begin{pmatrix} y_1(1) \\ y_1(2) \\ \vdots \\ y_1(l) \\ \vdots \\ y_{N_r}(l) \end{pmatrix} = \underbrace{\begin{pmatrix} \mathbf{s} & \mathbf{o} & \cdots & \mathbf{o} \\ \mathbf{o} & \mathbf{s} & \cdots & \mathbf{o} \\ \vdots & \vdots & \ddots & \vdots \\ \mathbf{o} & \mathbf{o} & \cdots & \mathbf{s} \end{pmatrix}}_{\mathbf{S}} \begin{pmatrix} h_{11} \\ h_{12} \\ \vdots \\ h_{1N_t} \\ \vdots \\ h_{N_rN_t} \end{pmatrix} + \mathbf{n} \tag{2.12}$$

Written in a closed form

$$\mathbf{y} = \mathbf{Sh} + \mathbf{n} \tag{2.13}$$

Each $\mathbf{s}$ is the following matrix

$$\mathbf{s} = \begin{pmatrix} s_1(1) & \cdots & s_{N_t}(1) \\ s_1(2) & \cdots & s_{N_t}(2) \\ \vdots & \vdots & \vdots \\ s_1(l) & \cdots & s_{N_t}(l) \end{pmatrix} \tag{2.14}$$

and $\mathbf{o}$ is $l \times N_t$ zero matrix. In other words, $\mathbf{S}$ is a bolck diagonal matrix with *block size* of $N_r \times N_r$, and each nonzero block is matrix $\mathbf{s}$ that represents the training symbols. The *element size* of the matrix $\mathbf{S}$ is thus $lN_r \times N_t N_r$. Equation (2.12) is an overdetermined system of linear equations that has an infinite number of solutions for $\mathbf{h}$. One of the most useful solutions is the least square solution

$$\hat{\mathbf{h}} = (\mathbf{S}^H \mathbf{S})^{-1} \mathbf{S}^H \mathbf{y} \tag{2.15}$$

where $\hat{\mathbf{h}}$ is an estimation of $\mathbf{h}$, $\mathbf{S}^H$ is the conjugate transpose of $\mathbf{S}$.

2.5.5 Equalization

Equalization can mitigate interchannel interferences and allow recovery of individual channels. If there are more equations than unknowns and if the channel matrix has full column rank, this system can be inverted to determine the unknowns. Transmitted symbols are recovered by *zero forcing* algorithm

$$\hat{\mathbf{x}} = (\mathbf{H}^H \mathbf{H})^{-1} \mathbf{H}^H \mathbf{y} \tag{2.16}$$

where $\hat{\mathbf{x}}$ is an estimation of $\mathbf{x}$, $\mathbf{H}^H$ is the conjugate transpose of $\mathbf{H}$.

Chapter 3

Basic investigations

This chapter focuses on SCM-SS scheme over nondispersive and dispersive channel. Condition number is introduced as a useful metric that determines the performance of MIMO communication systems. Noise enhancement mechanism is analyzed by singular value decomposition (SVD). Generation of single sideband optical field through Mach-Zehnder modulator (MZM) is given. Parameter dependences such as driving voltage of phase modulator, laser phase noise are discussed.

3.1 Transmission over nondispersive channel

Optical MIMO communications exhibit different characteristics and performance according to the propagation environment. Those characteristics have to be carefully taken into account. A nondispersive channel introduces no dispersion.

3.1.1 Nondispersive fiber link model

The channel impulse response between the ith receiver and the jth transmitter is denoted as g_{ij}. The channel is characterized by $\mathbf{G}(\tau;\, t)$. Assume an optical MIMO system

with $N_t = 2$ and $N_r = 2$. The mathematical description of a nondispersive channel is

$$\begin{pmatrix} U_1(t) \\ U_2(t) \end{pmatrix} = \begin{pmatrix} \cos\theta\,\delta(t) & \cos\left(\theta+\pi/2\right)\delta(t) \\ \sin\theta\,\delta(t) & \sin\left(\theta+\pi/2\right)\delta(t) \end{pmatrix} * \begin{pmatrix} E_1(t) \\ E_2(t) \end{pmatrix} \tag{3.1}$$

where $*$ represents convolution. Refer to Equation (2.4) for the meaning of $E_j(t)$. For brevity, Equation (3.1) can be written as

$$\mathbf{U}(t) = \mathbf{G}(\tau;\, t) * \mathbf{E}(t) \tag{3.2}$$

The coefficients of $\mathbf{G}(\tau;\, t)$ satisfy the requirement of power conservation, that is, the total power of each column is equal to one. Rewrite Equation (3.1) into equation group

$$\begin{cases} U_1(t) = \cos\theta\, E_1(t) + \cos\left(\theta+\pi/2\right) E_2(t) \\ U_2(t) = \sin\theta\, E_1(t) + \sin\left(\theta+\pi/2\right) E_2(t) \end{cases} \tag{3.3}$$

Upon square-law detection, the photo currents can be expressed as

$$\begin{cases} r_1(t) \propto \cos^2\theta \cos\Big(\omega_m t + \varphi_1(t)\Big) + \cos^2\left(\theta+\pi/2\right)\cos\Big(\omega_m t + \varphi_2(t)\Big) \\ r_2(t) \propto \sin^2\theta \cos\Big(\omega_m t + \varphi_1(t)\Big) + \sin^2\left(\theta+\pi/2\right)\cos\Big(\omega_m t + \varphi_2(t)\Big) \end{cases} \tag{3.4}$$

Turn Equation (3.4) to lowpass equivalent, and rewrite in matrix form

$$\begin{pmatrix} y_1(k) \\ y_2(k) \end{pmatrix} = \begin{pmatrix} \cos^2\theta & \cos^2\left(\theta+\pi/2\right) \\ \sin^2\theta & \sin^2\left(\theta+\pi/2\right) \end{pmatrix} \begin{pmatrix} x_1(k) \\ x_2(k) \end{pmatrix} + \begin{pmatrix} n_1(k) \\ n_2(k) \end{pmatrix} \tag{3.5}$$

Parameters for simulated transmission over nondispersive channel are shown in Table 3.1.

Table 3.1 Parameters for simulated transmission over nondispersive channel

Parameter	Value
number of Tx (N_t)	2
number of Rx (N_r)	2
frame size	127
training sequence	16
signature length	511
bit rate	1 Gbps
subcarrier frequency	4 GHz
chip rate	64 Gcps
sampling rate	256 GHz
halfwave voltage (V_π)	4.6 V
laser linewidth ($\Delta\nu$)	2 MHz

3.1.2 Condition number

Condition number is a metric that reflects the performance of MIMO communication system. To understand the meaning of condition number, Equation (2.11) is recalled. The condition number of $\mathbf{H}$ is defined as

$$\kappa(\mathbf{H}) = \| \mathbf{H} \| \| \mathbf{H}^{-1} \| \tag{3.6}$$

where $\| \mathbf{H} \|$ represents the norm of $\mathbf{H}$. Condition number can be calculated from a variety of matrix norms. For instance, Frobenius norm of $\mathbf{H}$ is defined as

$$\| \mathbf{H} \|_F = \sqrt{\sum_{i=1}^{N_r} \sum_{j=1}^{N_t} |h_{ij}|^2} \tag{3.7}$$

$\kappa(\mathbf{H}) \geq 1$ and when $\mathbf{H}$ is singular, that is, has no inverse matrix, $\kappa(\mathbf{H}) = +\infty$. The smaller the value of $\kappa(\mathbf{H})$, the more robust the solution of the system.

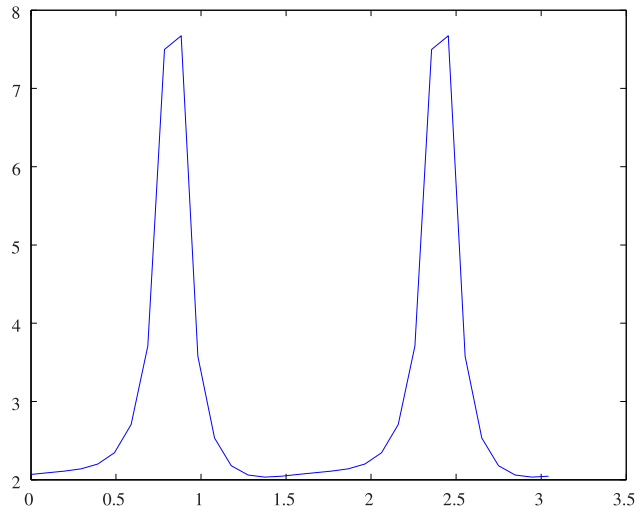

Figure 3.1 Spatial angle θ (rad) versus condition number.

Figure 3.1 shows the changing of condition number with respect to θ described in Equation (3.1). As θ approaches $\pi/4$, a pronounced peak was observed. Because of the additive noise, this inversion cannot give perfect estimates of the input symbols. In particular, when the channel matrix is ill-conditioned, estimation performance becomes poor because the channel inversion also enhances the noise.

3.1.3 Singular value decomposition

A *singular value* of the square or rectangular matrix $\mathbf{H}$ is a nonnegative scalar σ, and the pair of *singular vectors* u and v are two nonzero vectors so that

$$\mathbf{H}v = \sigma u$$
$$\mathbf{H}^H u = \sigma v \tag{3.8}$$

Written in matrix form, the defining equations for singular values and vectors are

$$\mathbf{HV} = \mathbf{U\Sigma}$$
$$\mathbf{H}^H\mathbf{U} = \mathbf{V\Sigma}^H \tag{3.9}$$

where $\mathbf{U} = [u_1, u_2, ..., u_r]$, $\mathbf{V} = [v_1, v_2, ..., v_r]$, $\mathbf{\Sigma} = diag(\sigma_1, \sigma_2, ..., \sigma_n)$, $\sigma_1 \geq \sigma_2 \geq ... \geq \sigma_n$, $\mathbf{\Sigma}^{-1} = diag(1/\sigma_1, 1/\sigma_2, ..., 1/\sigma_n)$. The matrices $\mathbf{U}$ and $\mathbf{V}$ are *unitary*, which satisfy $\mathbf{U}^H\mathbf{U} = \mathbf{I}$ and $\mathbf{V}^H\mathbf{V} = \mathbf{I}$. Consequently,

$$\mathbf{H} = \mathbf{U}\mathbf{\Sigma}\mathbf{V}^H \tag{3.10}$$

This is known as *singular value decomposition* (SVD). Condition number can also be expressed by the ratio between the largest and smallest singular values

$$\kappa(\mathbf{H}) = \| \mathbf{H} \| \| \mathbf{H}^{-1} \| = \sigma_1/\sigma_n \tag{3.11}$$

We will see that, the solution of a linear system can be analyzed by singular value decomposition

$$\begin{aligned} \hat{\mathbf{x}} &= \mathbf{H}^{-1}(b - n) \\ &= V\Sigma^{-1}U^H(b - n) \\ &= \sum_i \frac{v_i u_i^H}{\sigma_i} b - \sum_i \frac{v_i u_i^H}{\sigma_i} n \\ &= \mathbf{x} + \text{error} \end{aligned} \tag{3.12}$$

where $\hat{\mathbf{x}}$ means the estimation of $\mathbf{x}$. The discussion above is also called principal component analysis (PCA), which approximates a general matrix by a sum of a few simple matrices. As seen clearly from Equation (3.12), the error terms have a strong dependence on the singular values. Singular value decomposition unveils the noise enhancement mechanism of large condition number. As visualized in Figure 3.2, let θ vary in the range $[0, 90°]$. σ_2 is minimum when $\theta = 45°$. Use the relation in Equation (3.11), we can see that this result is in correspondence with that of Figure 3.1.

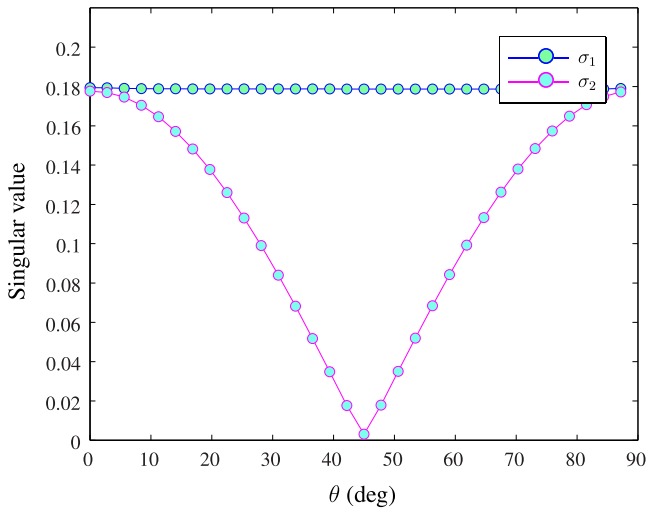

Figure 3.2 Singular values of channel matrix **H**.

3.1.4 Impact of phase offset in subcarrier

In Equation (3.4), the subcarrier phase offset of each channel is identical at the transmitter side. To investigate the impact of phase offset in subcarrier, a phase difference ϕ_d was intentionally introduced between the two channels, see Figure 3.3. Now the

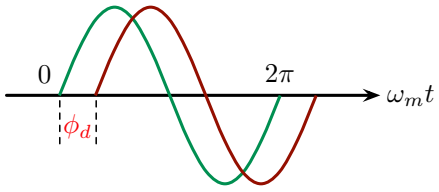

Figure 3.3 Introduce a phase difference between subcarrier offsets of the two channels.

transmitted optical fields can be written as

$$\begin{cases} E_1(t) = \exp\Big(i\omega_0 t + i\phi_1(t) + ic_1(t)\Big)\Big\{A_0 + A_m \exp\Big(i\omega_m t + i\varphi_1(t)\Big)\Big\} \\ E_2(t) = \exp\Big(i\omega_0 t + i\phi_2(t) + ic_2(t)\Big)\Big\{A_0 + A_m \exp\Big(i\omega_m t + i\varphi_2(t) + \phi_d\Big)\Big\} \end{cases} \tag{3.13}$$

where $E_1(t)$ and $E_2(t)$ are the input optical field of channel 1 and channel 2 respectively. The resultant photo currents can be written as

$$\begin{cases} r_1(t) \propto \cos^2\theta \cos\left(\omega_m t + \varphi_1(t)\right) + \cos^2\left(\theta + \pi/2\right) \cos\left(\omega_m t + \varphi_2(t) + \phi_d\right) \\ r_2(t) \propto \sin^2\theta \cos\left(\omega_m t + \varphi_1(t)\right) + \sin^2\left(\theta + \pi/2\right) \cos\left(\omega_m t + \varphi_2(t) + \phi_d\right) \end{cases} \tag{3.14}$$

The sampled (at symbol rate) lowpass equivalent of Equation (3.14) can be expressed in matrix form

$$\begin{pmatrix} y_1(k) \\ y_2(k) \end{pmatrix} = \begin{pmatrix} \cos^2\theta & \cos^2\left(\theta + \pi/2\right) e^{i\phi_d} \\ \sin^2\theta & \sin^2\left(\theta + \pi/2\right) e^{i\phi_d} \end{pmatrix} \begin{pmatrix} x_1(k) \\ x_2(k) \end{pmatrix} + \begin{pmatrix} n_1(k) \\ n_2(k) \end{pmatrix} \tag{3.15}$$

Let θ vary in the range $[0, 90°]$, and ϕ_d vary in the range $[0, 180°]$, the resultant condition number is illustrated in Figure 3.4. Compare Figure 3.4 to Figure 3.1, condition

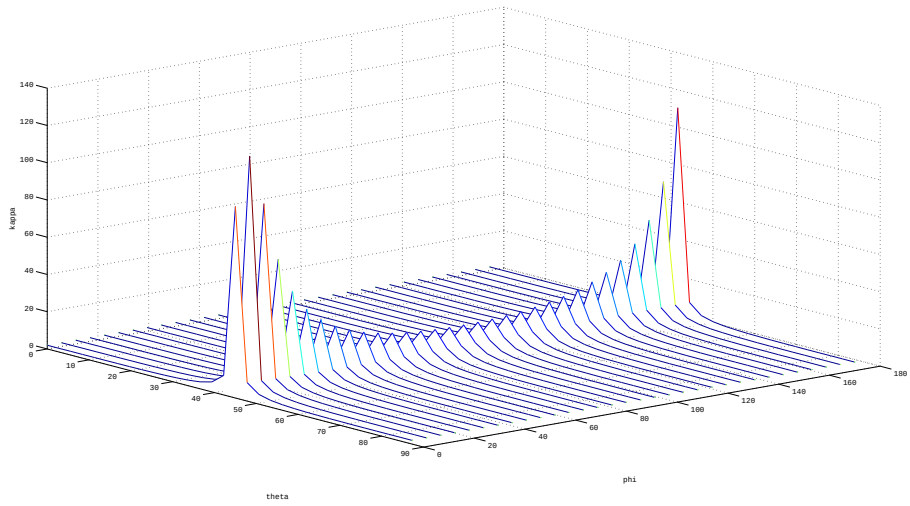

Figure 3.4 Condition number depends not only on amplitude, but also on phase.

number peaks are still observed, however, the peak values show a tendency of reducing by introducing an offset difference, especially under $\phi_d = 90°$, a minimum peak value was achieved.

3.1.5 Experimental transmission over nondispersive channel

Transmission over nondispersive channel is experimentally investigated.

Experimental setup

The experimental setup is illustrated in Figure 3.5. Experimental parameters are listed

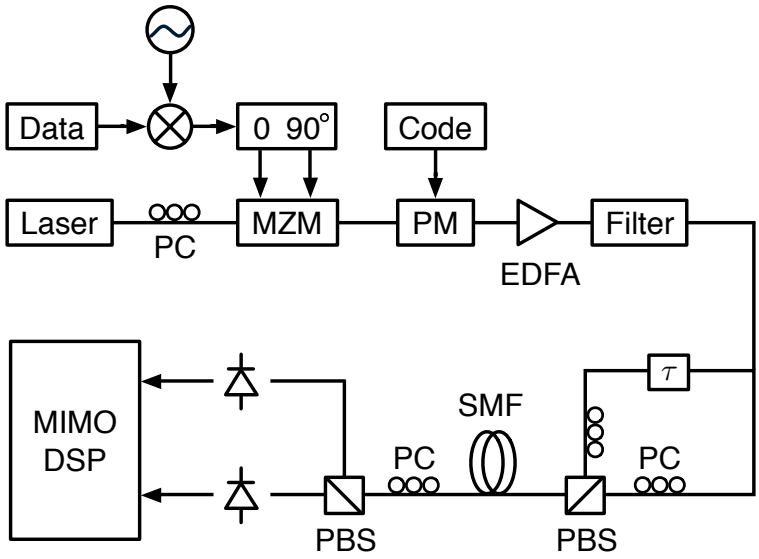

Figure 3.5 Experimental setup for 2×2 transmission over nondispersive channel.

in Table 3.2.

As mentioned in Section 2.4.1, SCM is to produce a modulated single sideband with an optical carrier. Optical SSB generation aims at compensating for the penalties brought by chromatic dispersion, as well as enhancing spectral efficiency. Multiple techniques are capable of implementing this type of optical field, such as optical heterodyning techniques, filtering methods and optical SSB modulators. In contrast to filters, OSSB modulators provide wavelength independent operation. SSB optical field is generated by using a dual-drive Mach-Zehnder modulator (MZM). The structure of Mach-Zehnder modulator is shown in Figure 3.6. RF subcarrier that carrying binary

Table 3.2 Parameters for experimental transmission over nondispersive channel

Parameter	**Value**
number of Tx (N_t)	2
number of Rx (N_r)	2
frame size	127
training sequence	16
signature length	511
bit rate	212.4834 Mbps
subcarrier frequency	3.069 GHz
chip rate	10 GHz
sampling rate	40 GHz
wavelength	1550 nm

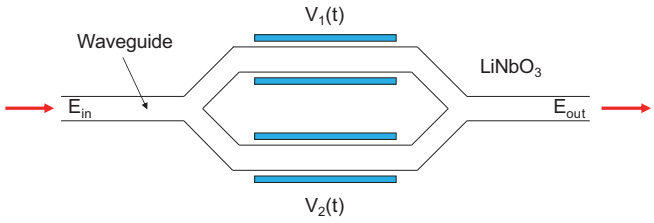

Figure 3.6 Structure of Mach-Zehnder modulator.

phase shift keyed (BPSK) data is split to two orthogonal arms by a 90° hybrid coupler. MZM is biased at quadrature point, and its two arms are modulated by the two orthogonal RF signals respectively. The dual-drive is biased at quadrature point, and the two arms are modulated by the two orthogonal electrical signals respectively. The resultant optical field forms a single sideband signal. The optical spectrum is broadened by *direct sequencing*, that is, optical field is phase modulated by spectrum-spreading code. The

optical field can be expressed as

$$E_j(t) = \exp\Big(i\omega_0 t + i\phi_j(t) + ic_j(t)\Big)\Big\{\exp\Big(i\beta\pi + i\alpha\pi\cos\big[\omega_m t + \varphi_j(t)\big]\Big) + \exp\Big(i\alpha\pi\cos\big[\omega_m t + \varphi_j(t) + \theta\big]\Big)\Big\} \quad (3.16)$$

where $\beta = (V_{dc}/V_\pi)$, V_{dc} is the DC bias voltage, V_π is the halfwave voltage of the MZM, $\alpha = (V_{ac}/V_\pi)$, V_{ac} is the amplitude of the RF signal, θ is the phase difference between the two arms of RF signals. Let $\beta = 1/2$ and $\theta = \pi/2$. Expanding Equation (3.16) according to Jacobi-Anger expansion and ignoring higher order harmonics yields

$$E_j(t) = \exp\Big(i\omega_0 t + i\phi_j(t) + ic_j(t)\Big)\Big\{\sqrt{2}J_0(\alpha\pi) \cdot \exp\big(i\pi/4\big) - 2J_1(\alpha\pi)\exp\Big(i\omega_m t + i\varphi_j(t)\Big)\Big\} \quad (3.17)$$

where J_0 and J_1 are the zeroth and first order Bessel functions of the first kind respectively, as can be seen from Figure 3.7. Equation (3.17) is the practical realization of

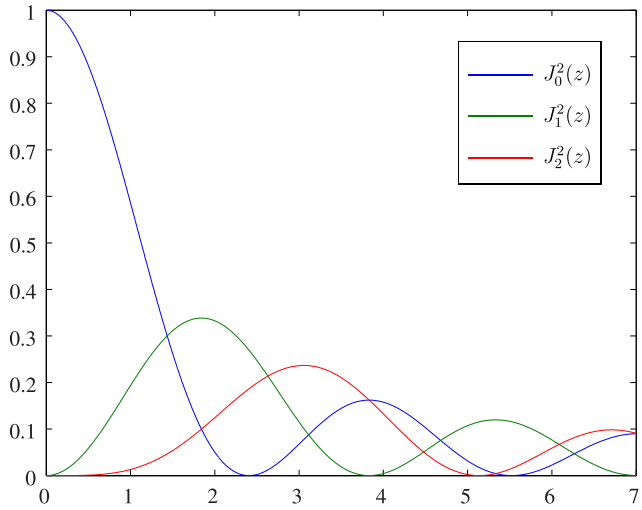

Figure 3.7 Bessel function of the first kind.

Equation (2.4).

An erbium-doped fiber amplifier (EDFA) is followed by a filter to eliminate the amplified spontaneous emission (ASE) noise. The optical field is split into two branches,

in order to generate two channels of signals. One of the branches is delayed by 1 km single mode fiber. Two channels are coupled to orthogonal polarizations of the PBS by adjusting polarization controllers, see Figure 3.8(a). Propagating through the single

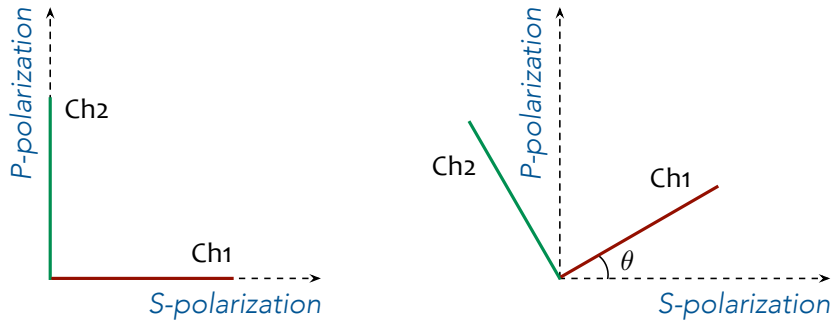

(a) (b)

Figure 3.8 (a) Two channels coupled to orthogonal polarizations of PBS. (b) Change the spatial angle θ, two channels overlapped on orthogonal polarizations of PBS.

mode fiber, which is a kind of nondispersive channel, the optical fields are projected to another PBS. Adjusting the polarization controller, equivalently to set the spatial angle θ, the two channels overlap on orthogonal polarizations of PBS, see Figure 3.8(b). Find the mathematical description in Equation (3.3). Coupled optical fields of two channels impinge on two photo detectors, one detector receives signals from S-polarization, and the other detector from P-polarization. Upon square-law detection, the electrical signals are sampled by A/D converter for off-line MIMO digital signal processing.

Experimental results

The recovered eye diagrams of two channels are shown in Figure 3.9. The spatial angle θ is approximately 30°.

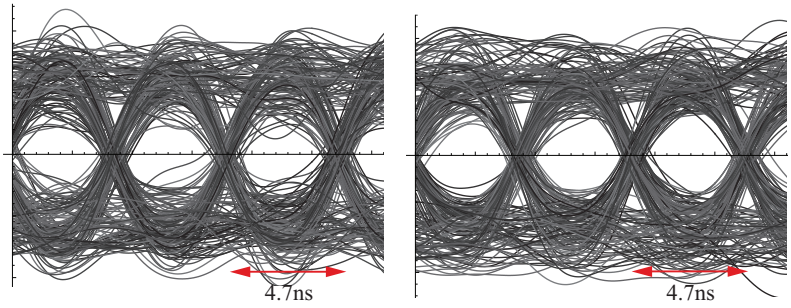

(a) Ch 1 (b) Ch 2

Figure 3.9 Eye diagrams of experimental transmission over nondispersive channel.

3.2 Transmission over dispersive channel

In Section 3.1, transmission over nondispersive channel has been investigated. In this section, few-mode fiber and multimode fiber link models are deduced. Physical characteristics of fiber channels are more involved. Dispersive channels manifest distinct behavior compared to nondispersive channels. Simulation of few-mode and multimode fiber links confirms the influence of modal dispersion.

3.2.1 Few-mode fiber link model

Few-mode fiber supports a few modes, generally two mode and four mode fibers are commercially available types. Assume the few-mode fiber link supports simultaneous transmission of four modes, namely, LP_{01}, LP_{12}, LP_{13} and LP_{21}. Of which LP_{01} is also called the fundamental mode. The fiber deployed is step index fiber with $r = 25\,\mu\mathrm{m}$, $\lambda = 1310\,\mathrm{nm}$, $n_1 = 1.480$, $n_2 = 1.465$. The mode power distribution of each mode seen from cross section of fiber core is shown in Figure 3.10. Propagation constants and corresponding mode delays of each mode are listed in Table 3.3. See Section 2.1.1 for their mathematical descriptions. A 2×2 MIMO transmission system is modeled as

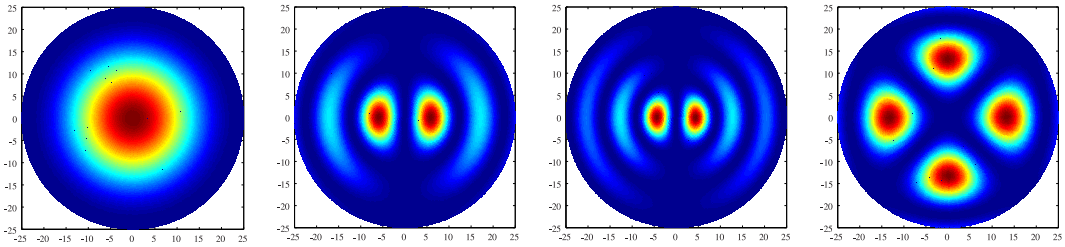

(a) LP01 (b) LP12 (c) LP13 (d) LP21

Figure 3.10 Fiber modes.

Table 3.3 Propagation constants and mode delays

Mode	$\boldsymbol{\beta}$ (μm^{-1})	$\boldsymbol{\tau}$ (ns/m)
LP_{01}	7.0377	4.8944
LP_{12}	7.0452	4.8996
LP_{13}	7.0587	4.9090
LP_{21}	7.0381	4.8947

$$\begin{pmatrix} U_1(t) \\ U_2(t) \end{pmatrix} = \begin{pmatrix} \cos\theta\,\delta(t-\tau_{11}) & \cos\left(\theta+\pi/2\right)\delta(t-\tau_{12}) \\ \sin\theta\,\delta(t-\tau_{21}) & \sin\left(\theta+\pi/2\right)\delta(t-\tau_{22}) \end{pmatrix} * \begin{pmatrix} E_1(t) \\ E_2(t) \end{pmatrix} \tag{3.18}$$

Rewrite Equation (3.18) into equation group

$$\begin{cases} U_1(t) = \cos\theta\,E_1(t-\tau_{11}) + \cos\left(\theta+\pi/2\right)E_2(t-\tau_{12}) \\ U_2(t) = \sin\theta\,E_1(t-\tau_{21}) + \sin\left(\theta+\pi/2\right)E_2(t-\tau_{22}) \end{cases} \tag{3.19}$$

The photo currents

$$\begin{cases} r_1(t) \propto \cos^2\theta\cos\Big(\omega_m t+\varphi_1(t)\Big) + \cos^2\left(\theta+\pi/2\right)\cos\Big(\omega_m t+\varphi_2(t)+\phi_d\Big) \\ r_2(t) \propto \sin^2\theta\cos\Big(\omega_m t+\varphi_1(t)\Big) + \sin^2\left(\theta+\pi/2\right)\cos\Big(\omega_m t+\varphi_2(t)+\phi_d\Big) \end{cases} \tag{3.20}$$

Sampled lowpass equivalent

$$\begin{pmatrix} y_1(k) \\ y_2(k) \end{pmatrix} = \begin{pmatrix} \cos^2\theta & \cos^2\left(\theta+\pi/2\right)e^{i\phi_d} \\ \sin^2\theta & \sin^2\left(\theta+\pi/2\right)e^{i\phi_d} \end{pmatrix} \begin{pmatrix} x_1(k) \\ x_2(k) \end{pmatrix} + \begin{pmatrix} n_1(k) \\ n_2(k) \end{pmatrix} \tag{3.21}$$

Parameters for simulated transmission over dispersive channel are listed in Table 3.4.

Table 3.4 Parameters for simulated transmission over dispersive channel

Parameter	**Value**
number of Tx (N_t)	2
number of Rx (N_r)	2
frame size	127
training sequence	16
signature length	511
bit rate	1 Gbps
subcarrier frequency	4 GHz
chip rate	64 Gcps
sampling rate	256 GHz
halfwave voltage (V_π)	4.6 V
laser linewidth ($\Delta\nu$)	2 MHz

3.2.2 Diversity to improve communication reliability

The prerequisite for MIMO to work is diversity. Diversity techniques have several benefits, such as more stable link quality, improved average performance, and in general these benefits are referred to as diversity gain. To illustrate the excess benefit of dispersive propagation environment that a single mode fiber cannot supply, back to back and different link distance transmissions are simulated.

Each channel couples fraction of the power to different modes, which propagate with different propagation constants, thus different group delays. Each photo detector collects different combination of optical power from different channels. Inter-modal coupling is allowable. Figure 3.11 demonstrate constellations of received and recovered signals under severe inter-modal coupling situation, to be specific, θ is set to 45° in Equation (3.18). Figure 3.11(a) shows the back to back transmission, obviously there

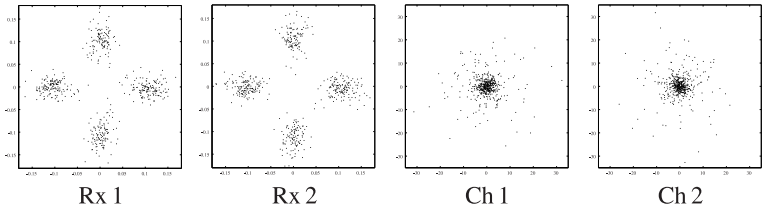

(a) Simulated back to back transmission (SCM-SS).

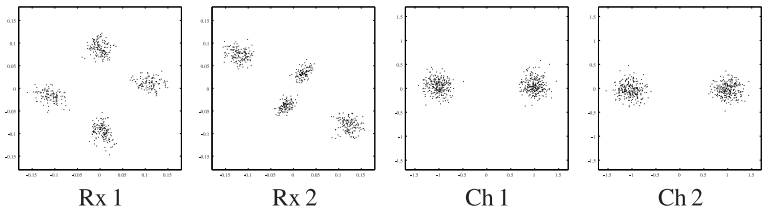

(b) Simulated transmission over 8 m four-mode fiber (SCM-SS).

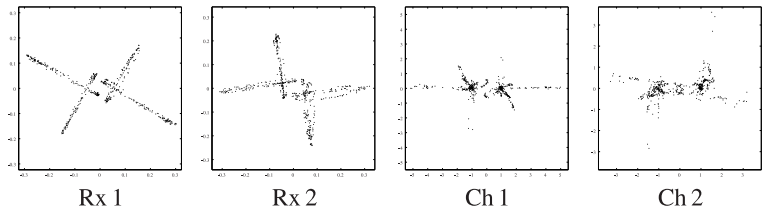

(c) Simulated transmission over 8 m four-mode fiber (SCM).

Figure 3.11 Constellation diagrams of simulated transmission over dispersive channel.

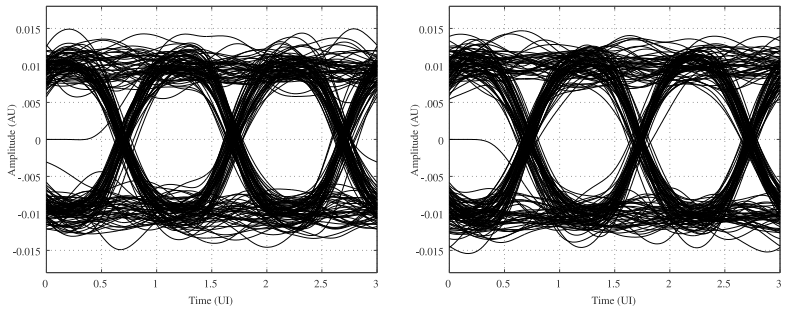

(a) Ch 1 (b) Ch 2

Figure 3.12 Eye diagrams of simulated transmission over 8 m four-mode fiber.

is no dispersion in this case. Figure 3.11(b) shows that after 8 m transmission, the transmitted data is successfully recovered. Figure 3.11(c) is the constellations of SCM scheme. No clear clusters can be identified. Figure 3.12 are corresponding eye diagrams of Figure 3.11(b).

3.2.3 Impact of laser phase noise

Laser phase noise is caused by spontaneous emission, and can be modeled as a Wiener process. It changes in a fast and random manner, and accumulates with the elapse of time.

$$var\left[\phi(t) - \phi(t-\tau)\right] = 2\pi\Delta\nu\tau \tag{3.22}$$

The linewidth of laser source can represent the strength of laser phase noise. Phase noises from different laser sources are preserved and converted to electrical domain. The influence of phase noise will corrupt the useful information bearing signal parts, making it difficult to track the channel. Impact of laser phase noise is explored numerically. The simulation configuration is visualized in Figure 3.13. The light sources of two

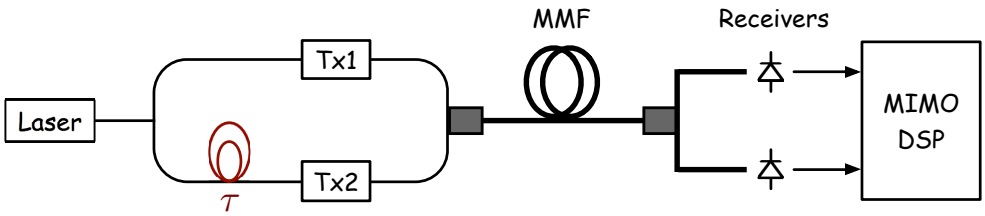

Figure 3.13 Decorrelated light source.

channels are derived from a single laser, which exhibits 2 MHz linewidth. The two light souces are decorrelated by a fiber delay line, beyond coherence length, they would become mutually incoherent light sources. The EVM performance of SCM and SCM-SS is illustrated in Figure 3.14. In Figure 3.14(a), the performance of SCM scheme

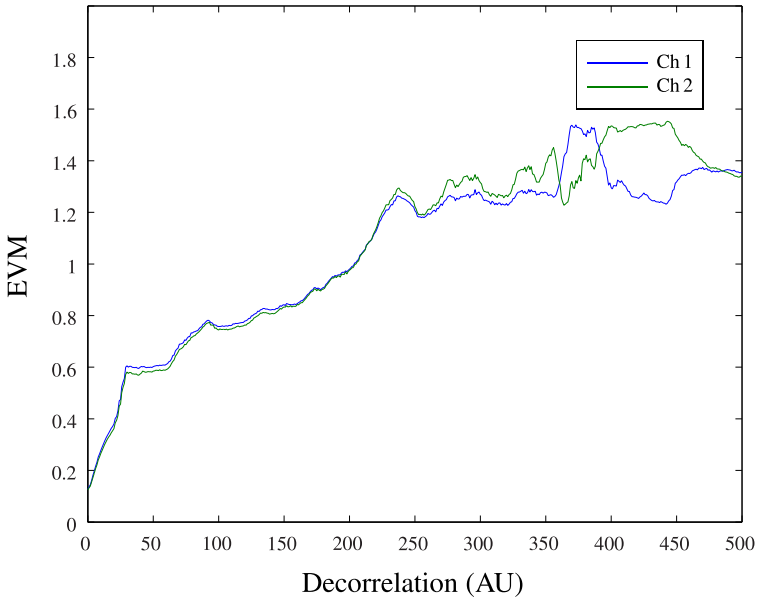

(a) SCM scheme.

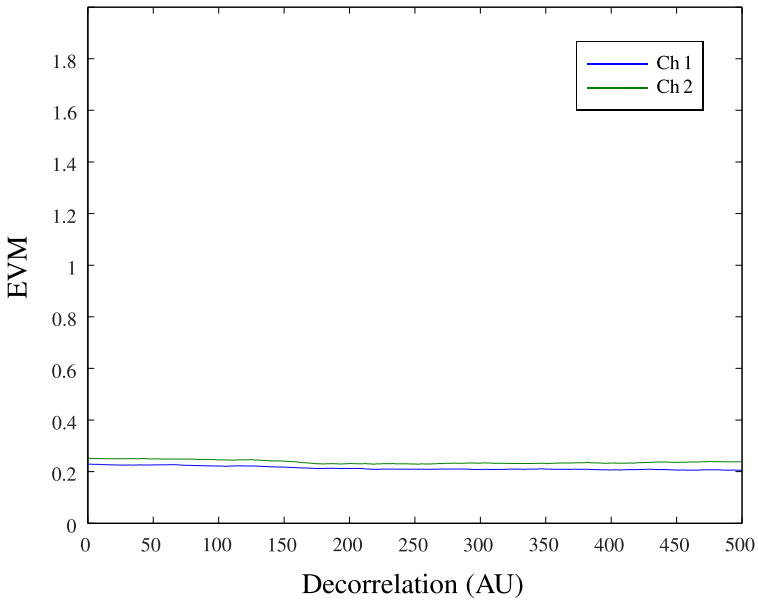

(b) SCM-SS scheme.

Figure 3.14 EVM performance versus decorrelation of light source.

degrades as the fiber delay line extends. On the contrary, in Figure 3.14(b), SCM-SS scheme is immune to laser phase noise. As mentioned before, the in-band phase noise terms are harmful, and the proposed scheme can spread the spectrum of phase noise containing terms, as a result, the residual in-band impairment is suppressed.

3.2.4 Statistical properties

Statistical properties are investigated by Monte Carlo simulation. For Monte Carlo simulation, under each θ in Equation (3.18), 10000 channel realizations are generated, that is, 10000 combinations of $\delta(t - \tau_{ij})$. Probability density function (PDF) and cumulative distribution function (CDF) of condition number are calculated based on the generated samples. The results are shown in Figure 3.15.

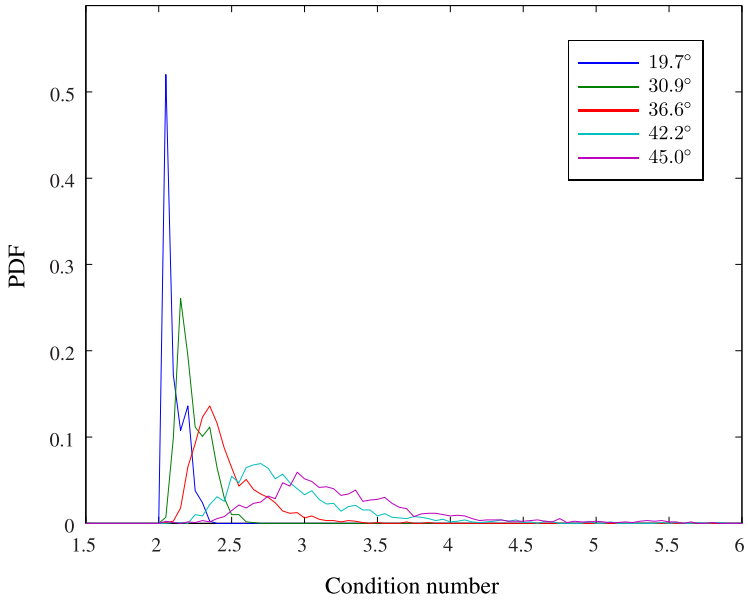

(a) Probability density function.

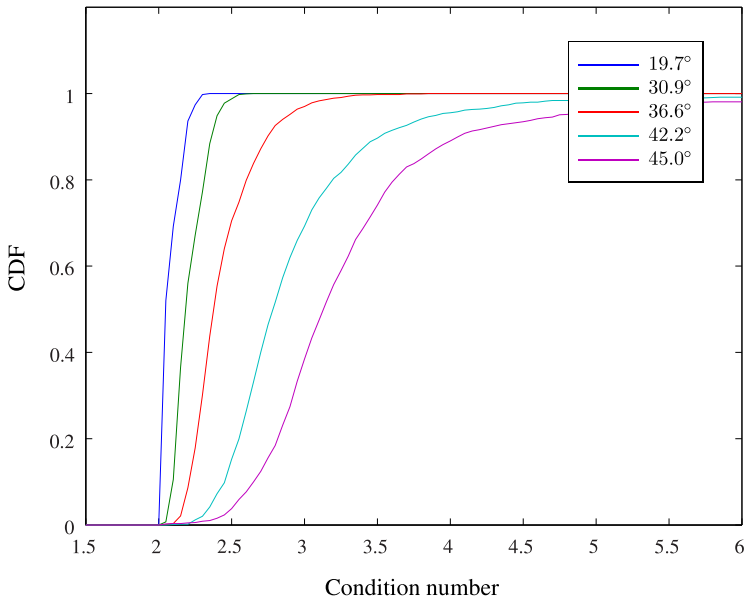

(b) Cumulative distribution function.

Figure 3.15 Condition number statistics.

3.2.5 Multimode fiber link model

Modeling of multimode fiber link is explored hereof. In a multimode fiber, the light propagates in a number of mode groups that travel in the fiber with different velocities, giving rise to intermodal dispersion. The modal bandwidth of the fiber, resulting from the intermodal dispersion, depends on launch conditions. Those conditions determine the amount of power launched into each of the mode groups, and, together with mode delays, determine the transfer function of the fiber. The mode delays can be calculated for a known fiber profile using the scalar wave equation. Similarly, one can compute the coupling coefficients (the fraction of total optical power launched into mode group) using the overlap integral. Without loss of generality, and to gain better insight into the problem, we assume that the mode attenuation is absent. Based on the discussion above, multimode fiber link can be described by impulse responses. The input facet of the fiber link is selective launched by each transmitter, and the output facet is selectively detected by each receiver, therefore spark off different impulse responses between each transmitter/receiver pair. Output optical field excited by the jth transmitter can be expressed as

$$\begin{aligned} E_{oj}(t) &= E_j(t) * g_j \\ &= E_j(t) * \sum_{k=1}^{P} a_{jk}\, \delta(t - \tau_k) \\ &= \sum_{k=1}^{P} a_{jk}\, E_j(t - \tau_k) \end{aligned} \tag{3.23}$$

where $E_j(t)$ is the input optical field from the jth transmitter, $*$ means convolution, g_j is the impulse response associated with the jth transmitter, P is the total number of modes supported by multimode fiber channel, a_{jk} is a multiplicative factor, the subscript jk means from the jth transmitter, via the kth mode, and τ_k is the group

delay for the kth mode. $\{a_{jk}\}$ exhibits a Gaussian profile. Gaussian pulse in time domain can be expressed as

$$a_{jk} = \frac{1}{\sigma_t\sqrt{2\pi}}\, e^{-\frac{(\tau_k-\tau_j^o)^2}{2\sigma_t^2}} \tag{3.24}$$

where τ_j^o is the group delay of the center mode for the jth transmitter, σ_t is the standard deviation in time domain. In frequency domain

$$H(f) = e^{-2\pi^2\sigma_t^2 f^2} \tag{3.25}$$

For half power, we have

$$e^{-2\pi^2\sigma_t^2 f_b^2} = 1/\sqrt{2} \tag{3.26}$$

Hence,

$$\omega_b = 2\pi f_b = \sqrt{\ln 2}/\sigma_t \Rightarrow \sigma_t = \sqrt{\ln 2}/\omega_b \tag{3.27}$$

Substituting $\sigma_t = \sqrt{\ln 2}/\omega_b$ to Equation (3.24) yields

$$a_{jk} = \frac{\omega_b}{\sqrt{2\pi\ln 2}}\, e^{-\frac{\omega_b^2(\tau_k-\tau_j^o)^2}{2\ln 2}} \tag{3.28}$$

Ignoring the coefficient, we have

$$a_{jk} = e^{-\frac{(\tau_k-\tau_j^o)^2}{2\sigma_t^2}} = e^{-\frac{\omega_b^2(\tau_k-\tau_j^o)^2}{2\ln 2}} \tag{3.29}$$

Assume the group delay of P modes supported by multimode fiber channel shows a linear dependence on the modal index $k \in N(1, P)$

$$\tau_k = k\Delta\tau \tag{3.30}$$

where $\Delta\tau$ is the delay increment between adjacent modes.

At the link end, the photo detectors perform selective detection of each channel. Each detector aims at collecting certain groups of modes. In other words, each detector has its own sensitivity or transfer function to each mode, which can be described as

$$b_{ik} = e^{-\frac{(\tau_k-\tau_i^o)^2}{2\sigma_t^2}} \tag{3.31}$$

where τ_i^o represents the time delay of the center mode for the ith receiver. When τ_i^o equals τ_j^o, it is the case that the ith receiver is perfectly matched to the jth transmitter. The impulse response between the ith receiver and the jth transmitter can be expressed as

$$g_{ij} = \sum_{k=1}^{P} b_{ik}\, a_{jk}\, \delta(t - \tau_k) \tag{3.32}$$

Parameters for simulated transmission over multimode fiber link are shown in Table 3.5. Figure 3.16 demonstrates the EVM performance versus $\Delta\tau$. Figure 3.17 exemplarily

Table 3.5 Parameters for simulated transmission over multimode fiber link

Parameter	**Value**
number of Tx (N_t)	4
number of Rx (N_r)	4
frame size	127
training sequence	16
signature length	511
bit rate	100 Mbps
subcarrier frequency	3.2 GHz
chip rate	12.8 Gcps
sampling rate	25.6 GHz
laser linewidth ($\Delta\nu$)	4 MHz

shows the received and recovered constellations when $\Delta\tau$ is around 15$\sim$20 ps.

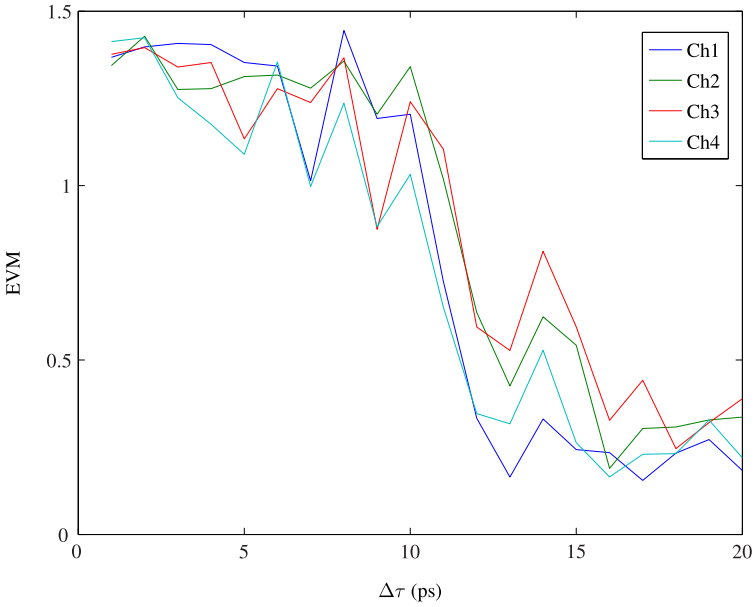

Figure 3.16 EVM performance versus $\Delta\tau$.

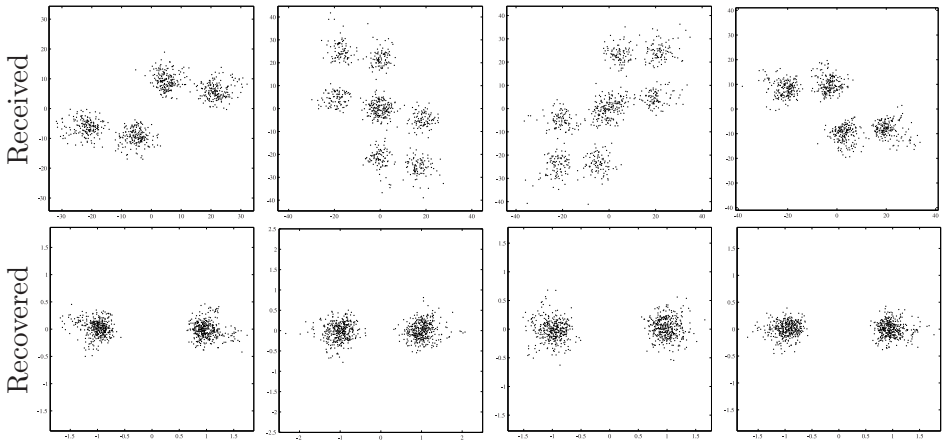

Figure 3.17 Constellations when $\Delta\tau$ is around 15∼20 ps.

3.2.6 Experimental transmission over dispersive channel

Transmission over dispersive channel is verified experimentally based on translation stage.

Experimental setup

Few-mode fiber link model is experimentally realized. The experimental setup is demonstrated in Figure 3.18. Dispersive propagation environment is implemented by con-

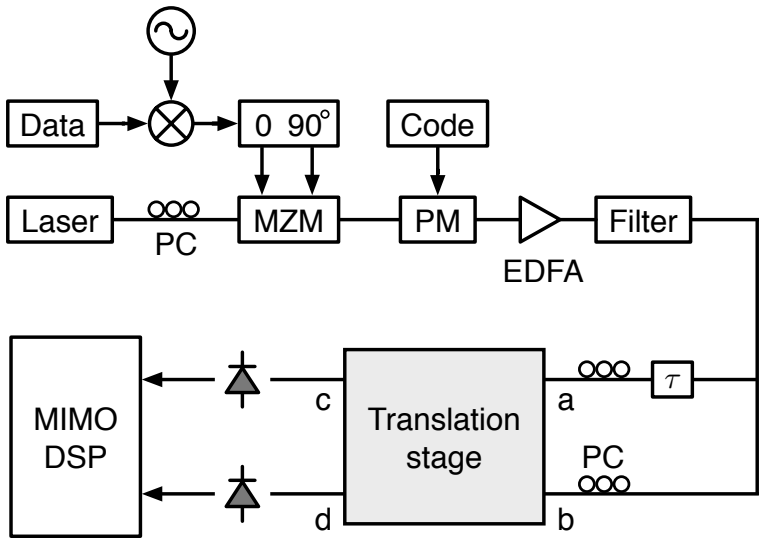

Figure 3.18 Experimental setup for 2×2 transmission over dispersive channel.

structing a translation stage. The detail of the translation stage is shown in Figure 3.19. Key components include polarization beam splitter, half mirror and collimator. The polarization beam splitter is a transparent cube consisting of two triangular prisms glued to each other, constructed to transmit horizontally polarized light, but reflect vertically polarized light. Beam splitter cubes and half mirrors are placed on the stage to form light paths with different lengths, which is a mimic of few-mode fiber. Differential path delay is introduced during propagation. Beam splitter cube splits incident

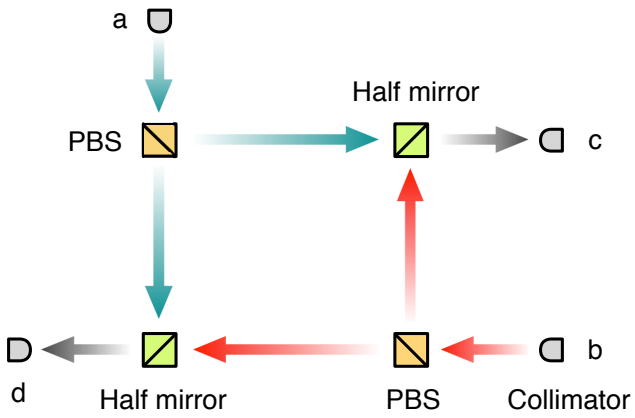

Figure 3.19 Configuration of translation stage.

optical field to p-polarization and s-polarization, half mirror is used to combine optical fields from different channels. Collimator will collect the combine optical fields, and feed to photo detector. Experimental parameters are tabulated in Table 3.6.

Table 3.6 Parameters for experimental transmission over dispersive channel

Parameter	**Value**
number of Tx (N_t)	2
number of Rx (N_r)	2
frame size	127
training sequence	16
signature length	2047
bit rate	100 Mbps
subcarrier frequency	2 GHz
chip rate	10 Gcps
sampling rate	20 GHz

Optimum phase modulator operating conditions

SCM-SS scheme utilizes spread spectrum technique to combat intermodal coupling induced impairment. As indicated in Equation (2.4), $c_j(t)$ is spreading code induced phase changing, phase modulator relies on Pockels effect to produce the phase changing, hence the applied driving voltage is vitally relevant to system performance, the influence is investigated numerically and experimentally. Figure 3.20(a) unveils the simulated results, and experimental results are shown in Figure 3.20(b). In Figure 3.20(a), the driving voltage is normalized by V_π, In order to verify the phase noise suppression ability further, the driving voltage of the phase modulator that modulated by the spreading code is controlled from 0 to $2V_\pi$, and the corresponding performance is evaluated by error vector magnitude (EVM). The horizontal axis represents driving voltage normalized by V_π. It is observed that in the region around V_π, the system achieved best performance.

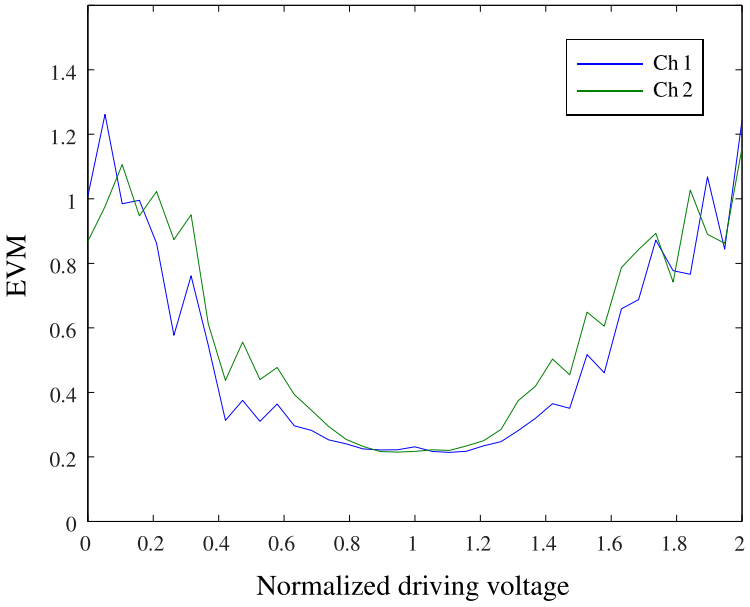

(a) Simulated.

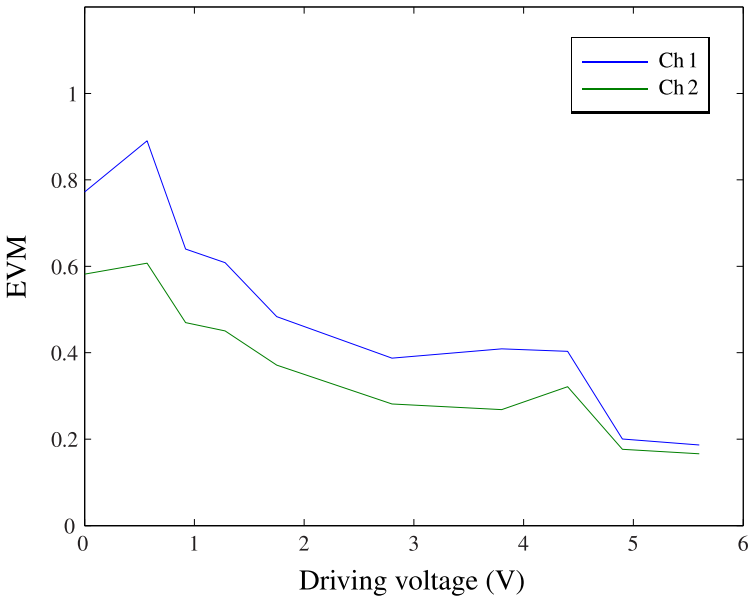

(b) Experimental.

Figure 3.20 EVM performance versus driving voltage.

Experimental results

The measured path power are $P_{ac} = -19.28\,\text{dBm}$, $P_{ad} = -17.53\,\text{dBm}$, $P_{bc} = -16.57\,\text{dBm}$, $P_{bd} = -20.96\,\text{dBm}$. Figure 3.21 shows the constellation diagrams of 2×2 transmission

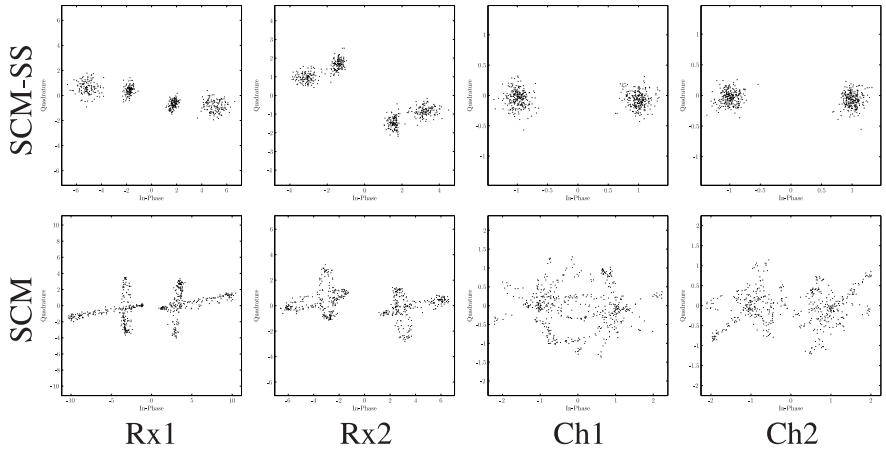

Figure 3.21 Constellation diagrams of 2×2 transmission over translation stage.

over translation stage. Figure 3.22 shows the eye diagrams of 2×2 transmission over translation stage. Condition number $\kappa(\mathbf{H}) = 2.7836$, EVM1 = 0.1865, EVM2 = 0.1661.

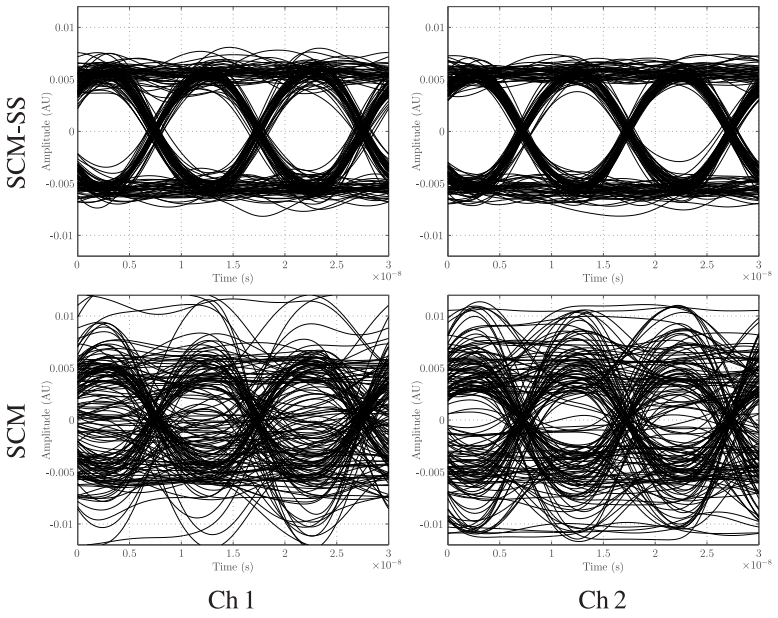

Figure 3.22 Eye diagrams of 2×2 transmission over translation stage.

Chapter 4

Transmission over multimode fiber links

As seen from Chapter 3, the feasibility and advantages of SCM-SS scheme have been confirmed numerically and experimentally. This chapter is dedicated to the experimental transmission over multimode fiber links.

4.1 2×2 transmission

2×2 transmission over multimode fiber links is conducted in this section.

Experimental setup

The experimental setup is shown in Figure 4.1. Corresponding parameters are shown in Table 4.1. A 1550 nm continuous wave DFB laser operates as the light source. SSB optical field is generated by using a dual-drive Mach-Zehnder modulator (MZM). RF subcarrier that carrying binary phase shift keyed (BPSK) data is split to two orthogonal arms by a $\pi/2$ hybrid coupler. MZM is biased at quadrature point, and its two arms are

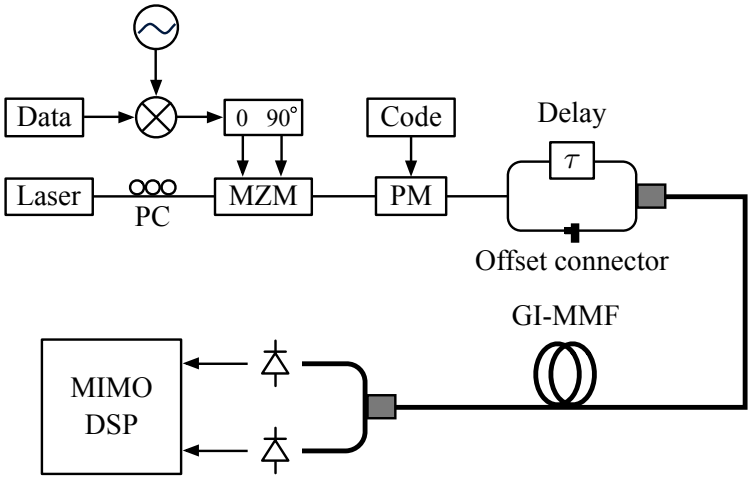

Figure 4.1 Experimental setup for 2×2 transmission over multimode fiber links.

Table 4.1 Parameters for 2×2 transmission over multimode fiber links

Parameter	**Value**
number of Tx (N_t)	2
number of Rx (N_r)	2
frame size	127
training sequence	16
signature length	2047
bit rate	100 Mbps
subcarrier frequency	2 GHz
chip rate	10 GHz
sampling rate	20 GHz
wavelength	1550 nm

modulated by the two orthogonal RF signals respectively. Such an optical field is then phase modulated by spectrum-spreading code. Erbium doped fiber amplifier (EDFA) is inserted to boost the power, and AWG filter eliminates the ASE noise. 3 dB coupler splits the light into two branches to form two channels. One of the branches is delayed by 2 km single mode fiber so as to decorrelate the two channels. The two channels carried by single mode fibers are coupled to the input ports of a fused multimode coupler through connectors. Of which one channel excites lower order modes by center launching, the other channel excites higher order modes by using an offset connector. The offset connector is equipped with a single mode fiber pigtail, with possible angular tilt and radial offset, the initial field of the multimode fiber input facet can be selectively excited. The fibers used are 50 μm core diameter graded index multimode fibers (GI-MMF). Different link lengths are constituted by 500 m and 1000 m fiber reels, which are connected by optical connectors. The output optical fields are directed to two photo detectors by another fused multimode coupler. Each detector receives a mixing of signals from both channels. The electrical signals are sampled by an A/D converter for off-line MIMO signal processing.

Experimental results

To confirm the advantages of the proposed SCM-SS scheme further, the experiments of SCM scheme that uses no spread spectrum technique are also conducted. Corresponding received and recovered constellations of 500 m transmission under both schemes are shown exemplarily in Figure 4.2. Figure 4.3 depicts eye diagrams of 500 m transmission under SCM-SS and SCM schemes for comparison. The widest eye opening was observed under SCM-SS scheme. Deterioration in eye opening of SCM scheme is attributed to in-band phase noise containing terms. 2×2 transmission experiments have been suc-

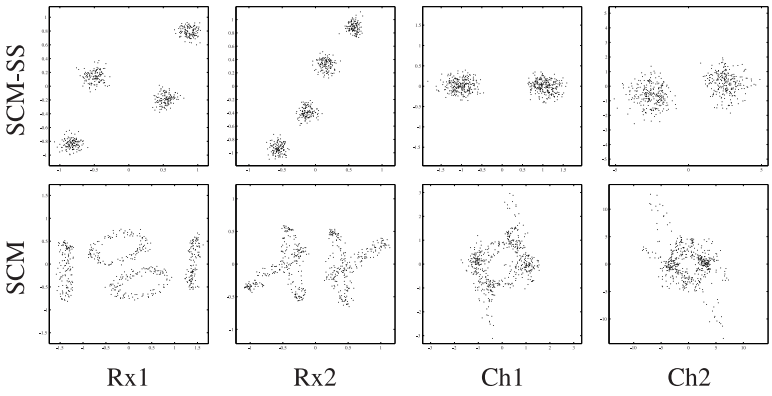

Figure 4.2 Constellation diagrams of 2×2 500 m transmission.

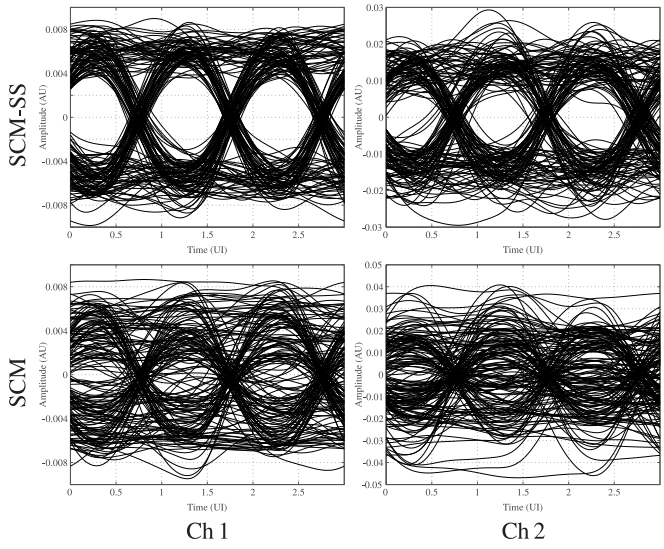

Figure 4.3 Eye diagrams of 2×2 500 m transmission

cessfully transmitted. However, the transmission performance is affected by the power distribution for each channel. Transmission over even longer distances is difficult, it is attributed to the self-interference phenomenon when too many higher order modes are excited, as analyed in Section 2.4.3.

4.2 2×4 transmission

From a statistical viewpoint, 2×4 MIMO can achieve higher diversity gain than 2×2 MIMO, which is thought to improve communication reliability. In all the following transmission experiments, offset connector is not used, because exciting of too many modes is not expected. Two groups of experiments are conducted.

4.2.1 Group I

Experimental setup

The experimental setup is shown in Figure 4.4. Corresponding parameters are shown

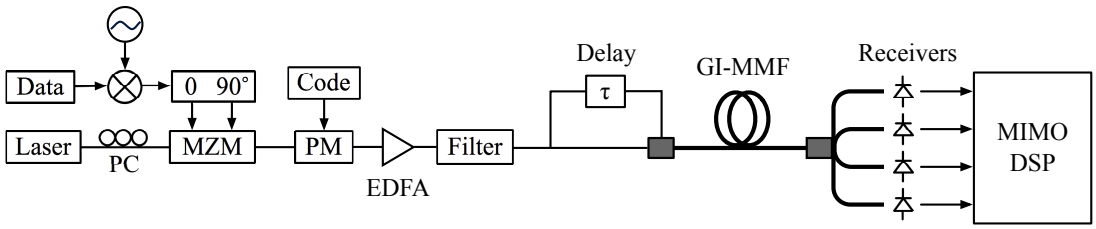

Figure 4.4 Experimental setup for 2×4 transmission over multimode fiber links.

in Table 4.2. A 1550 nm continuous wave DFB laser operates as the light source. SSB optical field is generated by using a dual-drive Mach-Zehnder modulator (MZM). RF subcarrier that carrying binary phase shift keyed (BPSK) data is split to two orthogonal arms by a $\pi/2$ hybrid coupler. MZM is biased at quadrature point, and its two arms are modulated by the two orthogonal RF signals respectively. Such an optical field is then

Table 4.2 Parameters for 2×4 transmission over multimode fiber links (Group I)

Parameter	**Value**
number of Tx (N_t)	2
number of Rx (N_r)	4
frame size	127
training sequence	16
signature length	2047
bit rate	100 Mbps
subcarrier frequency	2 GHz
chip rate	10 GHz
sampling rate	20 GHz
wavelength	1550 nm

phase modulated by spectrum-spreading code. Erbium doped fiber amplifier (EDFA) is inserted to boost the power, and AWG filter eliminates the ASE noise. 3 dB coupler splits the light into two branches to form two channels. One of the branches is delayed by 2 km single mode fiber so as to decorrelate the two channels. The two channels carried by single mode fibers are coupled to the input ports of a fused multimode coupler through connectors, which excite lower order modes of 50 μm core diameter graded index multimode fiber (GI-MMF) link. Different link lengths are constituted by 500 m and 1000 m fiber reels, which are connected by optical connectors. The output optical fields are directed to 4 photo detectors by another fused multimode coupler. Each detector receives a mixing of signals from both channels. The electrical signals are sampled by an A/D converter for off-line MIMO signal processing.

Experimental results

Figure 4.5 shows constellations diagrams for 2000m transmission of SCM and SCM-SS schemes. The eye diagrams are demonstrated in Figure 4.6. These cases are recovered

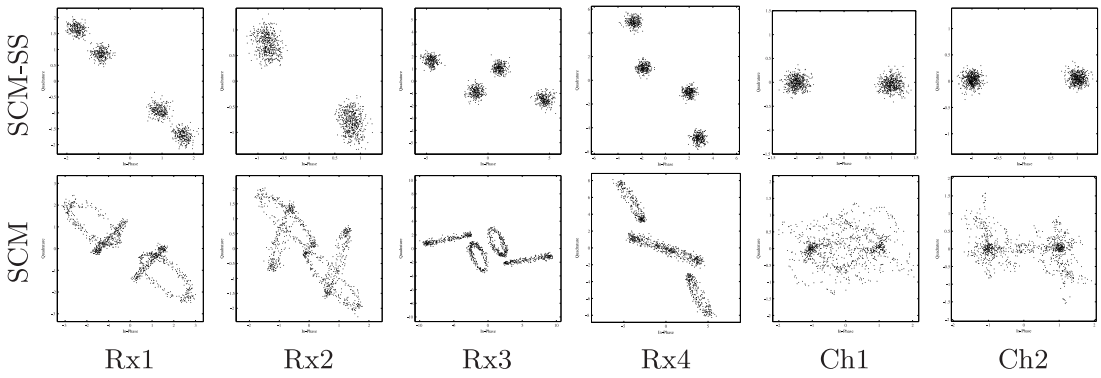

Figure 4.5 Constellation diagrams of 2×4 2000 m transmission (Group I).

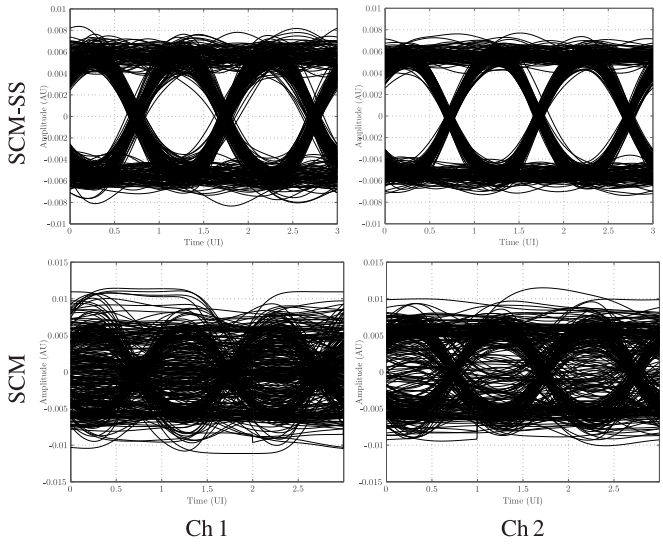

Figure 4.6 Eye diagrams of 2×4 2000 m transmission (Group I).

with SCM-SS while SCM scheme not. These results also indicate the advantage of proposed scheme. Figure 4.7 shows the error vector magnitude (EVM) for both schemes with different fiber length. The fiber lengths of 1500 m and 2000 m are consisted of 1000+500 m and 1000+500+500 m fibers, respectively. SCM-SS schemes achieve error

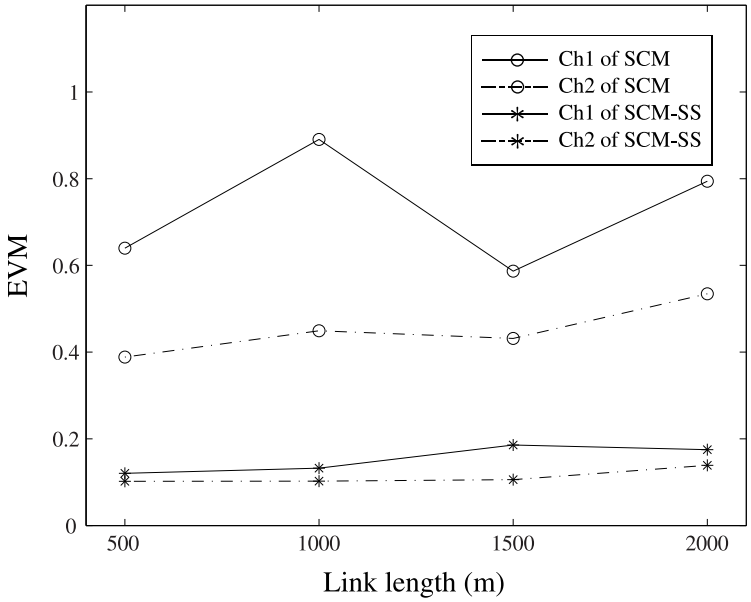

Figure 4.7 EVM of 2×4 transmission (Group I).

free operation and superior performance compared with SCM scheme is apparently exhibited through much lower EVM. When switching to different link lengths, fiber reels and connectors should be reorganized accordingly, though, stringent adjustments are not exercised, the requirements in alignment are shown to be loose.

Eigenvalue decomposition

Correlation matrix is defined as

$$\mathbf{G} = \mathrm{E}\left[\mathbf{H}^H\mathbf{H}\right] \tag{4.1}$$

where E[·] stands for expectation over all channel realizations. $\mathbf{G}$ is Hermitian and can be decomposed into product of three matrices by eigenvalue decomposition

$$\mathbf{G} = \mathbf{U}\mathbf{\Lambda}\mathbf{U}^H \tag{4.2}$$

where $\mathbf{U}$ is eigenvector matrix with orthonormal columns, and $\mathbf{\Lambda} = diag\left(\lambda_1, \lambda_2\right)$ is a diagonal matrix with real-valued, non-negative eigenvalues on the main diagonal.

eigenvalues are related to the channel capacity, which is calculated by

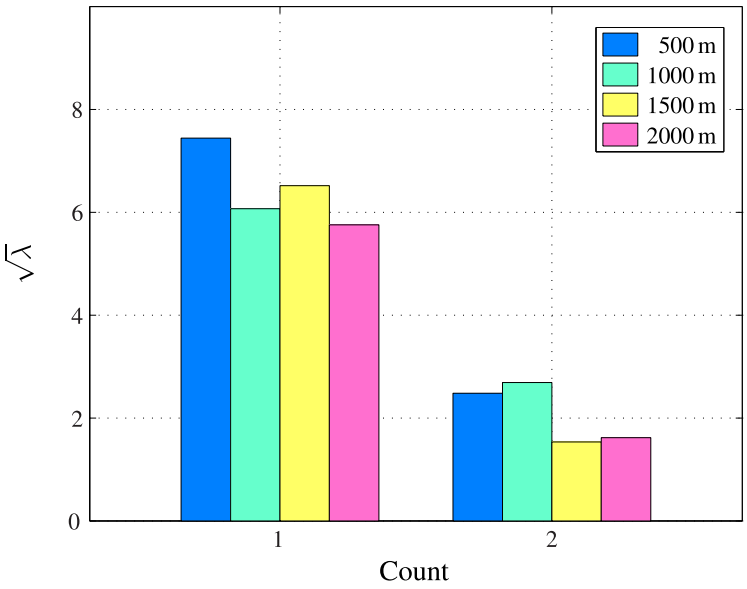

Figure 4.8 Eigenvalue decomposition (Group I).

$$C(\mathbf{H}) = B \cdot \mathrm{E}\left[\log_2 \left|\mathbf{I} + \frac{1}{\sigma^2}\mathbf{HRH}^H\right|\right] \tag{4.3}$$

where B is the bandwidth in Hertz, σ^2 is the variance of the noise elements. The covariance matrix $\mathbf{R}$ can also be chosen to maximize this capacity. [41]

4.2.2 Group II

Experimental setup

The experimental setup is shown in Figure 4.4. Corresponding parameters are shown in Table 4.3. In experiments 32 symbols of $2^9 - 1$ pseudo-random binary sequence (PRBS) are taken as training symbols, and $2^9 - 1$ symbols constitute one frame for each channel.

Table 4.3 Parameters for 2×4 transmission over multimode fiber links (Group II)

Parameter	Value
number of Tx (N_t)	2
number of Rx (N_r)	4
frame size	511
training sequence	16
signature length	32767
bit rate	100 Mbps
subcarrier frequency	2 GHz
chip rate	10 GHz
sampling rate	20 GHz

Experimental results

Up to 2000 m transmissions have been achieved via SCM-SS scheme. To confirm the advantages of the proposed SCM-SS scheme further, the experiments of SCM scheme that using no spread spectrum technique and IMDD-SS scheme are also conducted. Corresponding received and recovered constellations of 2000 m transmission under both schemes are shown exemplarily in Figure 4.9. Quantitative comparisons among them are given. The points of the SCM-SS scheme cluster closely, indicating good quality of signals, four clusters of points in the constellation diagram correspond to transmitted symbol pairs {1,1}, {1,-1}, {-1,1}, and {-1,-1}, meanwhile different styles of received constellations in SCM-SS scheme manifest modal-coupling diversity present at the output end of multimode fiber. Whereas the trajectories on the constellations of SCM scheme clearly reveal the influence of phase noises. Fig. 4.10 illustrates the error vector magnitude (EVM) of both schemes under different link lengths. Of which 1500 m

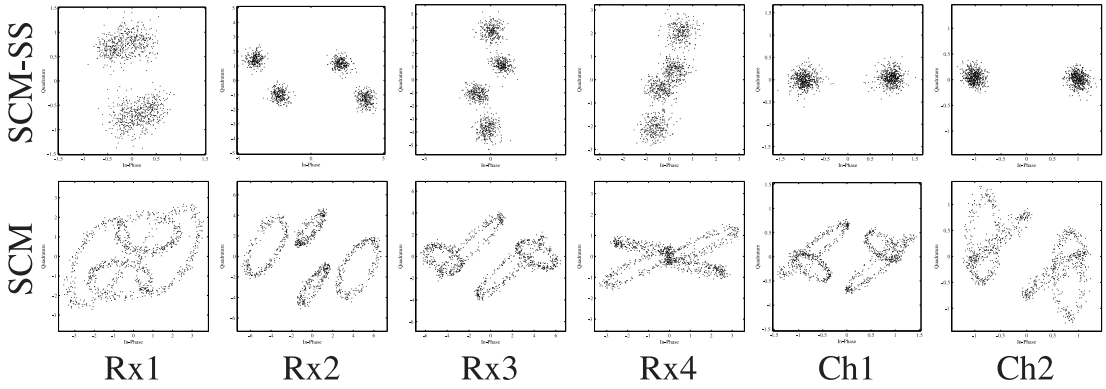

Figure 4.9 Constellation diagrams of 2×4 2000 m transmission (Group II).

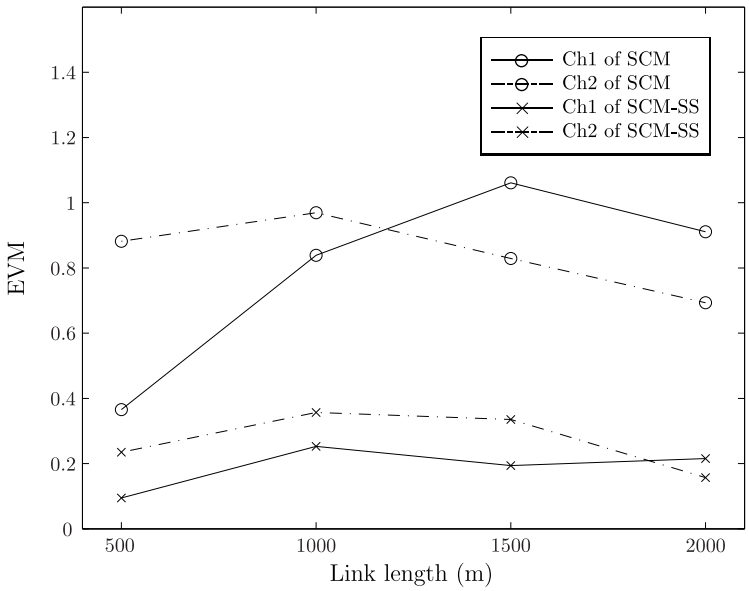

Figure 4.10 EVM of 2×4 transmission (Group II).

and 2000 m transmissions are comprised of 1000+500 m and 1000+500+500 m fibers respectively. Error free demodulation of SCM-SS scheme was verified, and superior performance compared with SCM scheme is apparently exhibited through much lower EVM. When switching to different link lengths, fiber reels and connectors should be reorganized accordingly, though, stringent adjustments were not exercised, manifesting the tolerances to channel fluctuations to some extent. To evaluate the performance further, the statistics of multimode fiber channel should also be taken into account [42]. Figure 4.11 depicts eye diagrams of 2000 m transmission under SCM-SS, SCM and

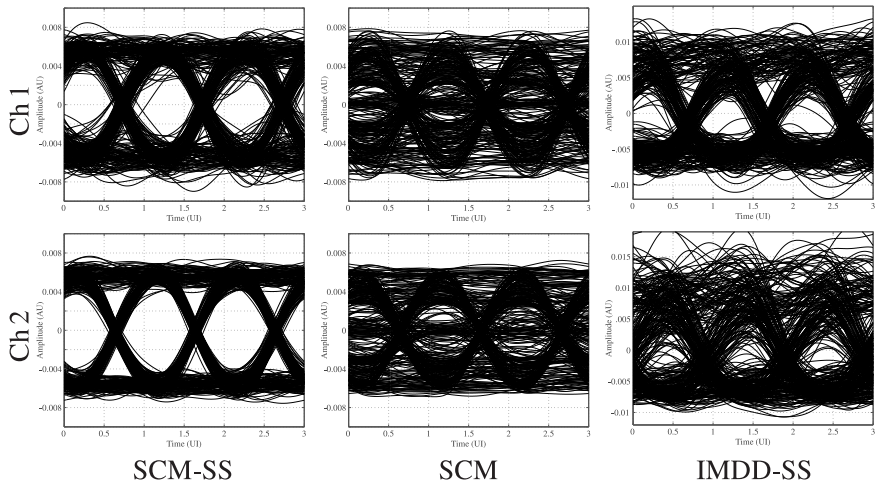

Figure 4.11 Eye diagrams of 2×4 2000 m transmission (Group II).

IMDD-SS schemes for comparison. The widest eye opening was observed under SCM-SS scheme. Deterioration in eye opening of SCM scheme is attributed to in-band phase noise containing terms. Slight eye opening can be observed in IMDD-SS scheme owing to the suppression of cross terms, though, inferior baseband environment and less degrees of freedom in channel matrix inhibit the further improvement in performance. Eigenvalue decomposition can be visualized in Fig. 4.12.

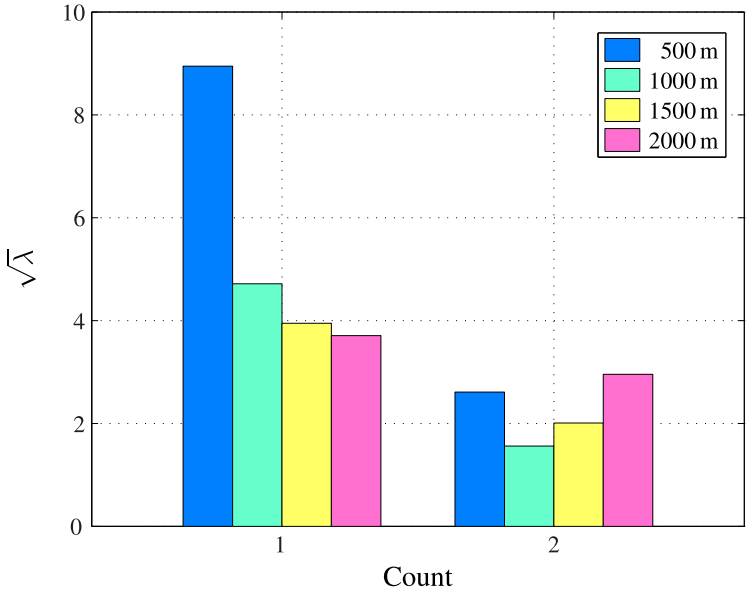

Figure 4.12 Eigenvalue decomposition (Group II).

4.3 4×4 transmission

As the number of channels increases, the required output power of light source also increases, which is challenging in practice. Also to couple the power of multiple channels with diversity,

Experimental setup

The experimental setup of 4×4 transmission is shown in Figure 4.13. Corresponding

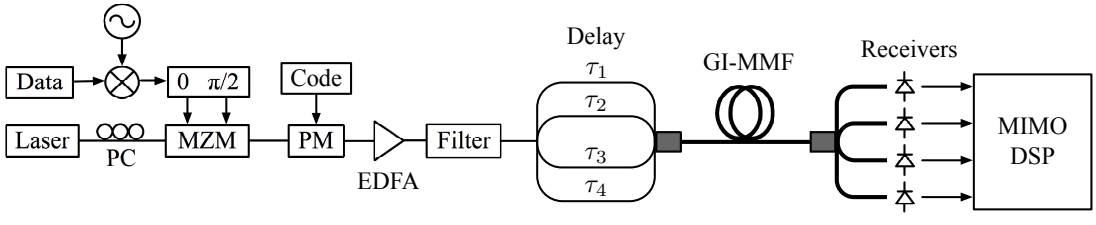

Figure 4.13 Experimental setup for 4×4 transmission over multimode fiber links.

parameters are shown in Table 4.4.

Table 4.4 Parameters for 4×4 transmission over multimode fiber links

Parameter	**Value**
number of Tx (N_t)	4
number of Rx (N_r)	4
frame size	511
training sequence	16
signature length	32767
bit rate	100 Mbps
subcarrier frequency	2 GHz
chip rate	10 GHz
sampling rate	20 GHz

Experimental results

Figure 4.14 shows constellation diagrams for 2000 m transmission of SCM-SS scheme. 2000 bits corresponding to less than 5×10^{-4} bit error rate is demonstrated. The

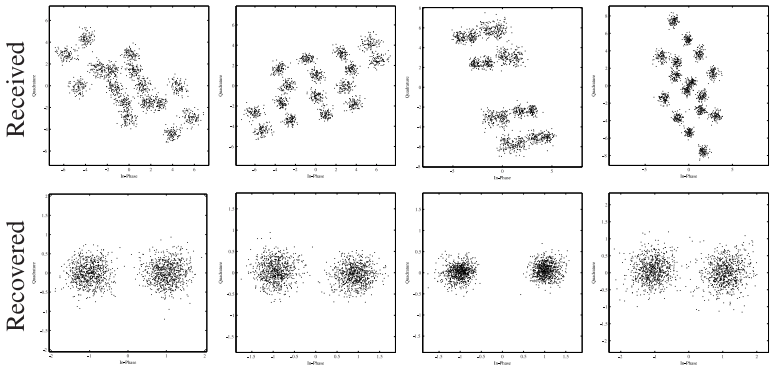

Figure 4.14 Constellation diagrams of 4×4 2000 m transmission.

results are affected by fiber transmission condition which is the power distribution for each modes and each receivers.

Chapter 5

Conclusions

5.1 Summary

SCM-SS scheme was proposed. Transmission over nondispersive and dispersive channel has been investigated. Condition number is introduced as a useful metric that determines the performance of MIMO communication systems. Noise enhancement mechanism is analyzed by singular value decomposition (SVD). Generation of single sideband optical field through Mach-Zehnder modulator (MZM) is given. 2×2, 2×4 and 4×4 transmissions have been experimental implemented over graded-index multimode fiber links. Satisfactory performance of optical MIMO using SCM-SS scheme is demonstrated in the presence of intermodal coupling, showing its applicability of capacity enhancement in multimode fiber links.

5.2 Outlooks

The group delay distribution are used to investigate differential mode delay (DMD) and EMBc. Mitigation of intersymbol interferences in wideband systems where the group

delay spread is comparable to the symbol period will be further studied. Intramodal dispersion such as chromatic dispersion, may also induce impairments to the transmission, although not a main concerning in multimode fiber channel. Compensation of these impairments leave us work to do.

To improve the data rate further, optical CDMA (OCDMA) is considered. To our knowledge, OCDMA using CW laser sources is encoded in electrical domain, optical domain implementation uses pulsed laser sources, the viability of incorporating in SCM-SS scheme remains to be convinced.

To evaluate the performance further, the statistics of multimode fiber channel should also be taken into account. Transmission performance over other types of fibers, such as few mode fiber, plastic optical fiber, etc., leaves us work to do.

References

[1] A. Chralyvy, "Plenary paper: The coming capacity crunch," in *Proc. Eur. Conf. Opt. Commun.*, Vienna, Austria, Sep. 2009.

[2] G. J. Foschini and M. Gans, "On limits of wireless communications in fading environments when using multiple antennas," *Wirel. Pers. Comm.*, vol. 6, pp. 311–335, Aug. 1998.

[3] C. P. Tsekrekos, A. Martinez, F. M. Huijskens, and A. M. J. Koonen, "Design considerations for a transparent mode group diversity multiplexing link," *IEEE Photon. Technol. Lett.*, vol. 18, no. 22, pp. 2359–2361, Nov. 2006.

[4] E. Ip, A. P. T. Lau, D. J. F. Barros, and J. M. Kahn, "Coherent detection in optical fiber systems," *Opt. Express*, vol. 16, no. 2, pp. 753–791, Jan. 2008.

[5] M. Nazarathy and A. Agmon, "Coherent transmission direct detection MIMO over short-range optical interconnects and passive optical networks," *J. Lightw. Technol.*, vol. 26, no. 14, pp. 2037–2045, Jul. 2008.

[6] P. J. Winzer and G. J. Foschini, "MIMO capacities and outage probabilities in spatially multiplexed optical transport systems," *Opt. Express*, vol. 19, no. 17, pp. 16 680–16 696, Aug. 2011.

[7] S. Randel, R. Ryf, A. Sierra, and P. J. Winzer, "6×56-Gb/s mode-division multiplexed transmission over 33-km few-mode fiber enabled by 6×6 MIMO equalization," *Opt. Express*, vol. 19, no. 17, pp. 16 697–16 707, Aug. 2011.

[8] T. Sakamoto, T. Mori, T. Yamamoto, and S. Tomita, "Differential mode delay managed transmission line for WDM-MIMO system using multi-step index fiber," *J. Lightw. Technol.*, vol. 30, no. 17, pp. 2783–2787, Sep. 2012.

REFERENCES

[9] T. Sakamoto, T. Mori, T. Yamamoto, and N. Hanzawa, "Mode-division multiplexing transmission system with DMD-independent low complexity MIMO processing," *J. Lightw. Technol.*, vol. 31, no. 13, pp. 2192–2199, Jul. 2013.

[10] M. Greenberg, M. Nazarathy, and M. Orenstein, "Data parallelization by optical MIMO transmission over multimode fiber with intermodal coupling," *J. Lightw. Technol.*, vol. 25, no. 6, pp. 1503–1514, Jun. 2007.

[11] R. E. Freund, C.-A. Bunge, N. N. Ledentsov, D. Molin, and C. Caspar, "High-speed transmission in multimode fibers," *J. Lightw. Technol.*, vol. 28, no. 4, pp. 569–586, Feb. 2010.

[12] M. Greenberg, M. Nazarathy, and M. Orenstein, "Performance of high-bitrate multiple-output links over multimode fiber with intermodal dispersion," *J. Lightw. Technol.*, vol. 26, no. 14, pp. 2192–2201, Jul. 2008.

[13] T. Uematsu, Y. Ishizaka, Y. Kawaguchi, K. Saitoh, and M. Koshiba, "Design of a compact two-mode multi/demultiplexer consisting of multimode interference waveguides and a wavelength-insensitive phase shifter for mode-division multiplexing transmission," *J. Lightw. Technol.*, vol. 30, no. 15, pp. 2421–2426, Aug. 2012.

[14] B. G. Lee, D. M. Kuchta, and F. E. Doany, "End-to-end multicore multimode fiber optic link operating up to 120 Gb/s," *J. Lightw. Technol.*, vol. 30, no. 6, pp. 886–892, Mar. 2012.

[15] J. M. Fini, B. Zhu, T. F. Taunay, and M. F. Yan, "Statistics of crosstalk in bent multicore fibers," *Opt. Express*, vol. 18, no. 14, pp. 15 122–15 129, Jul. 2010.

[16] J. Sakaguchi, Y. Awaji, N. Wada, and A. Kanno, "Space division multiplexed transmission of 109 Tb/s data signals using homogeneous seven-core fiber," *J. Lightw. Technol.*, vol. 30, no. 4, pp. 658–665, Feb. 2012.

[17] J. Sakaguchi, B. J. Puttnam, W. Klaus, and Y. Awaji, "305 Tb/s space division multiplexed transmission using homogeneous 19-core fiber," *J. Lightw. Technol.*, vol. 31, no. 4, pp. 554–562, Feb. 2013.

[18] B. Zhu, J. M. Fini, M. F. Yan, and X. Liu, "High-capacity space-division-multiplexed DWDM transmissions using multicore fiber," *J. Lightw. Technol.*, vol. 30, no. 4, pp. 486–492, Feb. 2012.

[19] J. M. Fini, B. Zhu, T. F. Taunay, M. F. Yan, and K. S. Abedin, "Statistical models of multicore fiber crosstalk including time delays," *J. Lightw. Technol.*, vol. 30, no. 12, pp. 2003–2010, Jun. 2012.

[20] X. Chen, A. Li, J. Ye, A. A. Amin, and W. Shieh, "Demonstration of few-mode compatible optical add/drop multiplexer for mode-division multiplexed superchannel," *J. Lightw. Technol.*, vol. 31, no. 4, pp. 641–647, Feb. 2013.

[21] M. Salsi, C. Koebele, D. Sperti, and P. Tran, "Mode-division multiplexing of 2×100 Gb/s channels using an LCOS-based spatial modulator," *J. Lightw. Technol.*, vol. 30, no. 4, pp. 618–623, Feb. 2012.

[22] R. Ryf, S. Randel, A. H. Gnauck, C. Bolle, A. Sierra, S. Mumtaz, and M. Esmaeelpour, "Mode-division multiplexing over 96 km of few-mode fiber using coherent 6×6 MIMO processing," *J. Lightw. Technol.*, vol. 30, no. 4, pp. 521–531, Feb. 2012.

[23] A. Li, A. A. Amin, X. Chen, S. Chen, G. Gao, and W. Shieh, "Reception of dual-spatial-mode CO-OFDM signal over a two-mode fiber," *J. Lightw. Technol.*, vol. 30, no. 4, pp. 634–640, Feb. 2012.

[24] I. B. Djordjevic, "Spatial-domain-based hybrid multidimensional coded-modulation schemes enabling multi-Tb/s optical transport," *J. Lightw. Technol.*, vol. 30, no. 24, pp. 3888–3901, Dec. 2012.

[25] W. Hofmann, N. H. Zhu, and M. Gorblich, "1.55-μm VCSEL arrays for optical multiple-input multiple-output (MIMO)," in *Proc. CLEO/IQEC*, 2009.

[26] J. Siuzdak, L. Maksymiuk, and G. Stepniak, "A 2 and 3 channel mode group diversity multiplexing transmission over graded and step index multimode fibers," in *Proc. Eur. Conf. Opt. Commun.*, Brussels, Belgium, Sep. 2008.

[27] G. Stepniak, L. Maksymiuk, and J. Siuzdak, "A mode group diversity multiplexing system for step and graded index multimode fibers," in *Proc. ICTON*, 2008.

[28] G. Stepniak, L. Maksymiuk, and J. Siuzdak, "Increasing multimode fiber transmission capacity by mode selective spatial light phase modulation," in *Proc. Eur. Conf. Opt. Commun.*, Torino, Italy, Sep. 2010.

[29] R. C. J. Hsu, A. Tarighat, A. Shah, A. H. Sayed, and B. Jalali, "Capacity enhancement in coherent optical MIMO (COMIMO) multimode fiber links," *IEEE Commun. Lett.*, vol. 10, no. 3, pp. 195–197, Mar. 2006.

[30] B. Jalali, R. C. J. Hsu, and A. R. Shah, "Coherent optical mimo," *Proc. of SPIE*, vol. 5814, pp. 121–127, 2005.

REFERENCES

[31] A. R. Shah, R. C. J. Hsu, and A. Tarighat, "Coherent optical MIMO (COMIMO)," *J. Lightw. Technol.*, vol. 23, no. 8, pp. 2410–2419, Aug. 2005.

[32] R. E. Tench, J.-M. P. Delavaux, L. D. Tzeng, R. W. Smith, L. L. Buhl, and R. C. Alferness, "Performance evaluation of waveguide phase modulators for coherent systems at 1.3 and 1.5 μm," *J. Lightw. Technol.*, vol. 5, no. 4, pp. 492–501, Apr. 1987.

[33] M. B. Shemirani, W. Mao, R. A. Panicker, and J. M. Kahn, "Principal modes in graded-index multimode fiber in presence of spatial- and polarization-mode coupling," *J. Lightw. Technol.*, vol. 27, no. 10, pp. 1248–1261, May 2009.

[34] C. P. Tsekrekos and A. M. J. Koonen, "Mitigation of impairments in MGDM transmission with mode-selective spatial filtering," *IEEE Photon. Technol. Lett.*, vol. 20, no. 13, pp. 1112–1114, Jul. 2008.

[35] L. G. Nielsen, Y. Sun, J. W. Nicholson, D. Jakobsen, R. L. Jr, and B. Palsdottir, "Few mode transmission fiber with low DGD, low mode coupling and low loss," in *Proc. Opt. Fiber Commun. Conf.*, 2012.

[36] B. C. Thomsen, "MIMO enabled 40 Gb/s transmission using mode division multiplexing in multimode fiber," in *Proc. Opt. Fiber Commun. Conf.*, 2010.

[37] C. P. Tsekrekos, "Mode group diversity multiplexing in multimode fiber transmission systems," Ph.D. dissertation, Eindhoven Univ. of Technology, Eindhoven, Jan. 2008.

[38] M. B. Shemirani and J. M. Kahn, "Compensation of multimode fiber dispersion by optimization of launched amplitude, phase, and polarization," *J. Lightw. Technol.*, vol. 28, no. 14, pp. 2084–2095, Jul. 2010.

[39] H. R. Stuart, "Dispersive multiplexing in multimode fiber," *Science*, vol. 289, no. 5477, pp. 281–283, Jul. 2000.

[40] B. Franz, D. Suikat, and R. Dischler, "High speed OFDM data transmission over 5 km GI-multimode fiber using spatial multiplexing with 2×4 MIMO processing," in *Proc. Eur. Conf. Opt. Commun.*, Torino, Italy, Sep. 2010.

[41] W. Weichselberger, M. Herdin, H. zcelik, and E. Bonek, "A stochastic MIMO channel model with joint correlation of both link ends," *IEEE Trans. Wireless Commun.*, vol. 5, no. 1, pp. 90–100, Jan. 2006.

[42] A. Tarighat, R. C. J. Hsu, and A. Shah, "Fundamentals and challenges of optical multiple-input multiple-output multimode fiber links," *IEEE Commun. Mag.*, vol. 45, no. 5, pp. 57–63, May 2007.

Appendix A

Jacobi-Anger expansion

In mathematics, the Jacobi-Anger expansion (or Jacobi-Anger identity) is an expansion of exponentials of trigonometric functions in the basis of their harmonics. It is useful in physics (for example, to convert between plane waves and cylindrical waves), and in signal processing (to describe FM signals). This identity is named after the 19th-century mathematicians Carl Jacobi and Carl Theodor Anger. The most general identity is given by

$$e^{iz\cos\theta} = \sum_{n=-\infty}^{\infty} i^n J_n(z) e^{in\theta} \tag{A.1}$$

and

$$e^{iz\sin\theta} = \sum_{n=-\infty}^{\infty} J_n(z) e^{in\theta} \tag{A.2}$$

where $J_n(z)$ is the nth Bessel function of the first kind. Using the relation $J_{-n}(z) = (-1)^n J_n(z)$, valid for integer n, the expansion becomes

$$e^{iz\cos\phi} = J_0(z) + 2\sum_{n=1}^{\infty} i^n J_n(z)\cos(n\theta) \tag{A.3}$$

This expansion represents an expansion of plane waves into a series of cylindrical waves. The derivation of Equation (3.17) takes advantage of Jacobi-Anger expansion.

APPENDIX A

Appendix B

Helmholtz equation

Multimode optical fiber is a type of optical fiber mostly used for communication over short distances, such as within a building or on a campus. The electric field in optical waveguides can be approximately described by the Helmholtz equation

$$\nabla^2\tilde{\mathbf{E}} + n^2(\omega)k_0^2\tilde{\mathbf{E}} = 0 \tag{B.1}$$

where the free-space wave number k_0 is defined as

$$k_0 = \omega/c = 2\pi/\lambda \tag{B.2}$$

and λ is the vacuum wavelength of the optical field oscillating at the frequency ω.

APPENDIX B

List of Figures

LIST OF FIGURES

List of Tables

LIST OF TABLES

Glossary

A/D	analog-to-digital
ASE	amplified spontaneous emission
Ch	channel
CW	continuous wave
DFB	distributed feedback
DSP	digital signal processing
EDFA	erbium-doped fiber amplifier
EVD	eigenvalue decomposition
GI	graded index
MDM	mode division multiplexing
MIMO	multiple-input multiple-output
MMF	multimode fiber
MZM	Mach-Zehnder modulator
PBS	polarization beam splitter

PC	polarization controller
PDM	polarization division multiplexing
PM	phase modulator
Rx	receiver
SCM	subcarrier multiplexing
SDM	space division multiplexing
SMF	single mode fiber
SS	spread spectrum
SVD	singular value decomposition
TDM	time division multiplexing
Tx	transmitter
WDM	wavelength division multiplexing

Acknowledgement

How time flies! I can clearly remember the scene when I just came to Kochi University of Technology, as it was yesterday.

Working toward a doctor's degree is not an easy thing. Hereby I am greatly indebted to my advisor Prof. Iwashita for his kindly guidance and encouragement on my research and study. Due to his enlightenment that I can enter this research field. Also I convey sincere gratitude to my vice advisors for their valuable suggestions and support.

I am grateful to the members of International Relations Center who gave me a great deal of help and assistance. And thanks to the Special Scholarship Program which provided me with a great opportunity to study abroad.

I am so thankful to my family who make me always surrounded by love. I owe special thanks to Mr. Guo for his waiting and understanding, which I will treasure up in my heart. I would like to acknowledge all my friends, and I will always cherish the memory with them.

Last but not least, I also feel obliged to the members of Iwashita Lab, and I will never forget the life in Kochi, in Japan.

ACKNOWLEDGEMENT

Publications

Journal papers

1) **Yang Zhang**, J. Matsushita, T. Nishimori, and K. Iwashita, "SCM-SS scheme for optical MIMO transmission using multimode fibers," *IEICE Commun. Express*, vol. 2, no. 6, pp. 268–273, Jun. 2013

2) **Yang Zhang** and K. Iwashita, "Design and performance of subcarrier multiplexing with spread spectrum scheme for optical MIMO transmission over multimode fiber links," *IEICE Trans. Commun.*, submitted.

Conferences

1) **Yang Zhang**, J. Matsushita, T. Nishimori, and K. Iwashita, "Optical MIMO with spread spectrum in multimode fiber transmission systems," in *Proc. IEICE General Conference*, Gifu, Japan, Mar. 2013

2) **Yang Zhang** and K. Iwashita, "MIMO transmission using SCM with modal diversity in multimode fiber systems," in *Proc. 10th International Conference on Optical Communications and Networks*, Guangzhou, China, Dec. 2011

3) T. Nishimori, **Yang Zhang**, J. Matsushita, and K. Iwashita, "A novel scheme for mode division multiplexed transmission by simultaneous transmission of local lights," in *Proc. Asia Communications and Photonics Conference*, Guangzhou, China, Nov. 2012